Chemical Papers (2022) 76:5655–5675
https://doi.org/10.1007/s11696-022-02273-2

ORIGINAL PAPER

Antioxidant activity and *α*-glucosidase inhibitability of *Distichochlamys citrea* M.F. Newman rhizome fractionated extracts: in vitro and *in silico* screenings

Tran Van Chen[1] · To Dao Cuong[2] · Phan Tu Quy[3] · Thanh Q. Bui[4] · Le Van Tuan[5] · Nguyen Van Hue[6] · Nguyen Thanh Triet[7] · Duc Viet Ho[8] · Nguyen Chi Bao[9] · Nguyen Thi Ai Nhung[4]

Received: 24 February 2022 / Accepted: 9 May 2022 / Published online: 1 June 2022

Abstract

Distichochlamys citrea M.F. Newman (commonly known as "Black Ginger") is an endemic plant to Vietnam and has been extensively exploited by folk medication for treatments of infection-related diseases and diabetes. In this work, its rhizomes were subjected to fractionated extraction, phytochemical examination, evaluation of antioxidant effect by DDPH free radical neutralization, and inhibitory activity toward *α*-glucosidase. The compositional components were subjected to in silico screening, including density functional theory calculation, molecular docking simulation, physicochemical analysis, and pharmacokinetic regression. In the trials, EtOAc fraction is found as the bioactive part of most effectiveness, regarding both antioxidant effect (IC_{50} = 90.27 μg mL^{-1}) and *α*-glucosidase inhibitory activity (IC_{50} = 115.75 μg mL^{-1}). Chemical determination reveals there are 13 components of its composition. DFT-based calculations find no abnormal constraints in their structures. Docking-based simulation provides order of inhibitory effectiveness: **3-P53341 > 12-P53341 > 7-P53341 > 4-P53341 > 11-P53341 > 10-P53341**. QSARIS-based investigations implicate their biocompatibility. ADMET-based regressions indicate that all candidates are generally safe for medicinal applications. The findings would contribute to the basis for further studies on the chemical compositions of *Distichochlamys citrea* and their biological activities.

Keywords *Distichochlamys citrea* · Antioxidant · *α*-glucosidase enzyme · Molecular docking simulation

Introduction

Diabetes mellitus (DM) is a chronic disease caused by a metabolic endocrine disorder in the body that is characterized by abnormally high levels of glucose in the blood (American Diabetes Association 2018). In its 10th edition, the International Diabetes Federation (IDF) has reported an estimated global prevalence of diabetes in the 20–79 age group of 10.5% (536.6 million) in 2021, and this number is expected to reach 12.2% (783.2 million) by 2045. Also in

✉ Nguyen Thanh Triet
nguyenthanhtriet1702@ump.edu.vn

✉ Nguyen Thi Ai Nhung
ntanhung@hueuni.edu.vn

[1] Faculty of Pharmacy, University of Medicine and Pharmacy at Ho Chi Minh City, Ho Chi Minh City 700000, Vietnam

[2] Phenikaa University Nano Institute (PHENA), Phenikaa University, Yen Nghia, Ha Dong District, Hanoi 12116, Vietnam

[3] Department of Natural Sciences and Technology, Tay Nguyen University, Buon Ma Thuot 630000, Vietnam

[4] Department of Chemistry, University of Sciences, Hue University, Hue City 530000, Vietnam

[5] Department of Environmental Science, University of Sciences, Hue University, Hue City 530000, Vietnam

[6] Faculty of Engineering and Food Technology, University of Agriculture and Forestry, Hue University, Hue City 530000, Vietnam

[7] Faculty of Traditional Medicine, University of Medicine and Pharmacy at Ho Chi Minh City, Ho Chi Minh City 700000, Vietnam

[8] Faculty of Pharmacy, Hue University of Medicine and Pharmacy, Hue University, Hue City 530000, Vietnam

[9] Hue University, Hue City 530000, Vietnam

this report, the IDF estimates that the prevalence of diabetes is expected to increase the most in middle-income countries (21.1%) compared to high-income (12.2%) and low-income countries (11.9%). Global diabetes-related health spending is estimated at $966 billion in 2021 and this number is projected to reach $1.054 billion by 2045 (Sun et al. 2022).

Diabetes mellitus can be classified into two most common groups: type 1 diabetes mellitus (which is characterized by the destruction of pancreatic β-cells), type 2 diabetes mellitus (which is characterized by combinations of decreased insulin secretion and peripheral insulin resistance). Diabetes mellitus might be due to a genetic abnormality, other pathologic disorders, clinical conditions, or gestational diabetes mellitus (Draznin et al. 2022). Among diabetic patients, type 2 diabetes mellitus is the most prevalent type of diabetes, accounting for 90–95% (Henning 2018). Type 2 diabetes mellitus patients are more susceptible to different forms of complications, e.g., cardiovascular diseases (hypertension, hyperlipidemia, heart attacks, coronary artery disease, strokes, cerebral vascular disease, and peripheral vascular disease), nephropathy, retinopathy, neuropathy, and cancers (Wu et al. 2014; Sandholm and Forsblom 2020).

Oxidation is a normal and regular process in the body. However, increased production of reactive oxygen species (ROS; e.g., hydroperoxyl, superoxide, hydrogen peroxide, and hydroxyl radicals) and reactive nitrogen species (RNS) (Newsholme et al. 2016; Yaribeygi et al. 2020) explicitly leads to oxidative stress, disrupting the balance between the activity of the free radicals and antioxidative systems of the body cells and tissues. The agents can oxidize proteins, lipids, and nucleic acids to produce toxic by-products, which in turn result in cellular damages, including structural alterations in membranes, organelle injury, DNA damage, and cell dysfunction (Yaribeygi et al. 2020; Radi et al. 2018). Over time, oxidative stress inevitably causes many serious diseases, e.g., diabetes, chronic inflammation, hypertension, dyslipidemia, and atherosclerosis (Ito et al. 2019). Oxidative stress is among the most apparent factors associated with metabolic diseases and diabetes mellitus progression, which are consistent with an increased prevalence of secondary diabetic complications (Newsholme et al. 2016; Oguntibeju 2019). Therefore, antioxidant therapy is often recommended as an effective approach to preventing complications of diabetes and its related diseases. Also, there has been increasing solid evidences on the relation between pre-historic diabetes and severe complications induced by COVID-19 (Gregory et al. 2021). However, glycemic parameters changed for the worse in patients with type 2 diabetes during the lockdown (Eberle and Stichling 2021). In addition, the increasing prevalence of diabetes is due to the aging population (Sun et al. 2022), obesity, and unhealthy lifestyle (such as sedentary lifestyle, physical inactivity, smoking, and alcohol consumption) (Wu et al. 2014).

The α-glucosidase enzyme is an essential enzyme of digestion that stimulates the break-down of disaccharides and oligosaccharides into small, simple, and absorbable carbohydrates (Tomasik and Horton 2012). α-glucosidase belongs to the group of enzymes that catalyze the release of α-glucose from non-reduced ends of α-glucosides or from complex polymers with α-(1–4) bonds. The enzymes are widely found in various kinds of organisms, e.g., bacteria, fungi, plants, and animals. They can be classified into two or three groups depending on their primary structures or substrate specificities (Moral et al. 2018). Based on the similarity of gene sequences, the enzymes are mainly divided into two families: GH-family 13 and 31. *Saccharomyces cerevisiae* α-glucosidases belong to GH-family 13 which is typical for bacteria and insects (Dušan et al. 2014; Costa-Latgé et al. 2021). The removal of the glucose molecules from N-glycans (Glc3Man9GlcNAc2) of glycoproteins in the endoplasmic reticulum is performed by two different types of α-glucosidases produced by *Saccharomyces cerevisiae*, viz. Glucosidase 1 (Gls1) and Glucosidase 2 (Gls2) (Hossain et al. 2016). The 3D structure of α-glucosidase MAL12 extracted from *Saccharomyces cerevisiae* had been well-determined and was published to UniProt under the entry ID P53341.

α-glucosidase inhibitors (AGIs) are a group of antidiabetic drugs used for the management of type 2 diabetes mellitus, e.g., acarbose, voglibose, and miglitol. AGIs inhibit the enzyme α-glucosidase at the intestinal epithelium, thus delaying the absorption of carbohydrates from the small intestine, particularly useful for reducing postprandial blood glucose (Akmal and Wadhwa 2021). Acarbose is the most commonly used drug in this group. It has been shown to stabilize blood glucose, increase life, and reduce the risk of cardiovascular development in patients with type 2 diabetes mellitus due to its ability against oxidative stress and endothelial dysfunction (DiNicolantonio et al. 2015).

Compared with synthesized drugs, the use of herbs for the treatment of diabetes is perceived to have a high economic value and fewer side effects. Currently, many groups of pharmaceutical drugs are used to treat type 2 diabetes, e.g., biguanides, sulphonylureas, thiazolidinediones, DPP-4 (dipeptidyl peptidase-4) inhibitors, SGLT2 (sodium-glucose cotransporter 2) inhibitors, GLP-1 RAs (glucagon-like peptide 1 receptor agonists), and Meglitinides (glinides) (Draznin et al. 2022). Recently, pharmaceutical drugs have often only played a role in blood glucose control. Due to the long-term treatment according to the regimen, these drugs are expensive and they can be associated with many harmful side effects for patients. For instance, SGLT2 inhibitors cause urinary-genital infections, and ketoacidosis (Moradi-Marjaneh et al. 2019); GLP-1 RAs can cause nausea, vomiting, diarrhea (Reid 2013; Sun et al. 2015), injection-site reactions, and

pancreatitis (Reid 2013). In folk experiences, many types of herbs have been used for a long time. These herbs have good effects on improving diabetes symptoms and are more affordable, with fewer side effects compared to synthetic drugs (Alam et al. 2018). Based on previous studies, bioactive compounds of plant origin, e.g., phenolic compounds, phytosterols, alkaloids, terpenoids, flavonoids, or glycosides, have shown anti-allergic, anti-cancer, antibacterial, anti-inflammatory, anti-diabetic, and antioxidant activities (Blahova et al. 2021). These compounds may also contribute to improved insulin sensitivity by hampering oxidative stress.

The genus *Distichochlamys* of the family Zingiberaceae is a genus endemic that is native to Vietnam, particularly first described by M.F.Newman in (1995). *Distichochlamys citrea* M.F. Newman (also known as "Black Ginger") has been discovered in Thua Thien Hue, Quang Binh, Quang Tri, Quang Nam, and Nghe An (Ty et al. 2017; Huong et al. 2017). *Distichochlamys citrea* was a small herb with 38–48 cm high, elongated rhizome, green leaves, and yellow flowers (Newman 1995). In Vietnam, there are preceding studies reporting the chemical composition of *Distichochlamys citrea* leaves and rhizomes, including essential oil with active constituents, such as 1.8-cineole, α-citral, β-citral, geraniol, geranyl acetate, terpinen-4-ol, linalool, and α-terpineol (Ty et al. 2017; Huong et al. 2017). The found substances hold certain important roles in the health benefits and prevention of illnesses, including anticancer, anti-inflammatory, antioxidant, antibacterial activities, etc. (Moteki et al. 2002; Quintans-Júnior et al. 2011). Although the genus *Distichochlamys* is of great interest to many researchers, there have been not many published studies on other chemical components. In particular, to the best of our knowledge, there is no publication on the biological activities of *Distichochlamys citrea* in Vietnam and worldwide. According to the experience of the Pa Kô people (A Lưới District, Thua Thien Hue Province), *Distichochlamys citrea* is known especially effective for the treatment of infection-related diseases, and diabetes.

In silico technique, based on computational simulation and computing calculation, is currently seeing a gain in popularity for medical science as prescreening research. It is for reducing the cost and time of wet laboratory experiments by predicting the compounds with undesirable properties and the most promising candidates. The former substances are deemed to be eliminated from the next analysis or further-developed research, while the latter justifies the selection. (Ferreira et al. 2015) Regarding ligand–protein interaction, molecular docking simulation is an effective method to investigate the potency of a ligand as an inhibitor toward its targeted protein. The method can estimate ligand-target binding energy and intermolecular interaction, thus predicting the static stability of the inhibitory systems.(Kapetanovic 2008) Specification to drug design for diabetes, molecular docking technique demonstrated its contributive significance regarding a variety of ligand families.

In this work, experiments were carried out to find evidences for the antioxidant and anti-diabetic activities of *Distichochlamys citrea* M.F. Newman fractionated extracts; while, computations were designed for the screening of α-glucosidase inhibitability of compositional components, in particular, and their bio-pharma compatibilities, in general. The former includes spectroscopic characterizations (GC–MS and bioassays), and the latter was a combination of quantum chemical properties (DFT calculation), intermolecular inhibitability (molecular docking simulation), physicochemical (QSARIS) and pharmacological (ADMET) compatibilities. This is the first experiment-computation effort on the bioactive investigation of *Distichochlamys citrea* M.F. Newman fractionated extracts.

Methodology

Experimentation

Material

Plant material The plant used in this study was collected in October 2019 from Bach Ma National Park, Thua Thien Hue Province, Vietnam. The scientific name (binomial nomenclature) of the plant was identified by Assoc. Prof. Truong Thi Bich Phuong (Department of Biology, University of Sciences, Hue University). The study sample was profiled by DNA-based identification and approved for submission by GenBank under the code MZ310840.1 (https://www.ncbi.nlm.nih.gov/nuccore/MZ310840.1). A voucher specimen (sample code: DC-10.19) was stored at the laboratory of Traditional Medicine, Faculty of Traditional Medicine, University of Medicine and Pharmacy in Ho Chi Minh City, Vietnam. After harvesting, the samples were removed gravelly and washed using tap freshwater. These samples were dried at room temperature, avoiding sunshine for 5–7 days, ground into a midding powder (1.0 kg), and chemically extracted. The collected extracts were used for examination in this research. Morphological characteristics of *Distichochlamys citrea* M.F. Newman with all parts of the plants are shown in Fig. 1.

Material for in vitro assay Chemicals and reagents: ethanol (OPC Pharmaceutical Company); *n*-hexane, *n*-butanol, ethyl acetate (VN-Chemsol, Co.Ltd); methanol, dimethylsulfoxide (DMSO) (Merck Co.Ltd, Germany); *p*-nitrophenyl-α-D-glucopyranoside (*p*-NPG), 2.2-diphenyl-1-picrylhydrazyl (DPPH), ascorbic acid, α-glucosidase from *Saccharomyces cerevisiae* (Sigma Co.Ltd, USA); acarbose (Chemcruz,

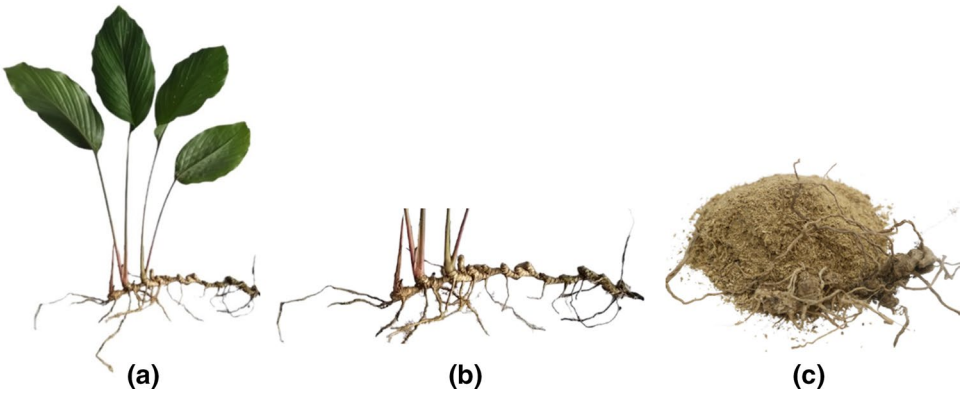

Fig. 1 All parts of the plants **a**, fresh root and rhizome **b**, dried power rhizomes **c** of *Distichochlamys citrea* M.F. Newman were collected in Bach Ma National Park, Thua Thien Hue Province

Santa Cruz Biotechnology, Inc., USA). All other chemical reagents used in this study were of analytical grade.

General experimental procedures

Preliminary phytochemical screening The preliminary phytochemical study was performed by the Ciulei method (C.I Methodology of Analysis of Vegetable and Drugs 1984) with slight modification. The phytochemical constituents, such as carbohydrates, essential oil, fats, amino acids, sterols, tannins, flavonoids, alkaloids, coumarins, cardiac glycosides, saponins, and polyuronides were analyzed qualitatively using the standard protocol. The powder samples were extracted with diethyl ether, ethanol, and finally distilled water so that extracts were obtained.

Pharmacognostic evaluation Pharmacognostic parameters (moisture content, total ash value, and acid-insoluble ash of dried powder) of rhizome powder were determined accordingly to the methods recommended by the Vietnamese Pharmacopoeia V (House and Vietnamese Pharmacopoeia 2017). The experiment was in triplicate and the results were expressed as mean values ± SD (Standard Deviation).

Preparation of crude and fractionated extracts The powder sample was tested for purity, preliminary investigation of phytochemical, and extracted with 96% ethanol (EtOH) by percolation and liquid–liquid method distribution (with solvents of increasing polarity being *n*-hexane, chloroform ($CHCl_3$), ethyl acetate (EtOAc), *n*-butanol (*n*-BuOH), respectively) to obtain total extract and respective fractions. All the solvent was recovered by a rotary evaporator at 45 ± 5 °C to obtain crude and fractionated extracts of *Distichochlamys citrea* rhizomes. The moisture content of the crude and fractionated extracts was determined using a Mettler Toledo scale. These concentrated extracts were stored at 4 °C in a refrigerator for further biological screenings. The fractionated extract with the strongest antioxidant and α-glucosidase inhibitory activities was analyzed by Gas chromatography-mass spectrometry (GC–MS). The chemical structures of this extract's main constituents were then used as the input for the evaluation of α-glucosidase inhibitory activity by in silico implementations.

GC–MS analysis Gas chromatography-mass spectrometry (GC–MS) was chosen for compositional analysis, especially to identify high-volatile components of the extracts. The performance was on the Agilent GC 7890B-MS 5975C instrument equipped with Agilent DB-5MS capillary column (30 m × 0.25 mm × 0.25 µm); Operating configuration: MS transfer line temperature (280 °C), ion source temperature (230 °C), EI mode (70 eV), mass scan range (29–650 amu). Helium was used as the carrier gas with a constant flow rate of 1.5 mL.min^{-1}. The fractionated extract of 1.0 µL was injected with a 20:1 split ratio into the GC. The column temperature was started at 80 °C for 1 min (isothermal) then increased linearly to 300 °C at the rate of 20 °C min^{-1} (for 15 min) with the inlet temperature set at 250 °C. The components of fractionated extract were identified based on their mass spectrometry data by comparison with NIST-17 MS database.

Antioxidant assay by DPPH inhibition The antioxidant capability of fractionated extracts was determined using DPPH (2,2-Diphenyl-1-picrylhydrazyl) radical scavenging activity method described by Mošovská et al. (2015) with improving adjustments (Mošovská et al. 2015). Ascorbic acid was used for positive control, which was prepared with a range of concentrations, i.e., 1.38, 2.75, 5.50, 11.01, 22.02 µg mL^{-1} (eq. Initial concentration: 62.5, 125.0, 250.0, 500.0, 1000.0 µM). Dilute 0.6 mM DPPH reagent in MeOH. The fractionated extracts were dissolved in methanol solution and diluted to get sample concentrations ranging from 31.25, 62.5, 125.0, 187.5, and 250 µg mL^{-1}. The reaction mixture in methanol consists of 0.5 mL of sample solution of different concentrations in reaction with 3.0 mL of 0.6 mM DPPH solution, afterward adding methanol until yielding 4.0 mL total volume of solutions. The mixture was

incubated in dark at room temperature for 30 min. Methanol 4.0 mL was used as a blank. Meanwhile, the control was a mixture of 3.5 mL methanol with 0.5 mL 0.6 mM DDPH solution. After the reaction, the sample absorbance was measured by ultraviolet–visible spectroscopy (UV–VIS) at a wavelength of 517 nm. The scavenging efficiency of free radicals is assessed through the color change from purple to yellow.

The antioxidant activity was determined using the following formula:

$$\text{Free radical scavenging activity (\%)} = \frac{\text{Control absorbance} - \text{Sample absorbance}}{\text{Control absorbance}} \times 100$$

The antioxidant activity of fractionated extracts was expressed by IC_{50} value (μg mL^{-1}). The fractionated extracts were prepared in a series of 5 various concentrations. Using Microsoft excel software to plot the dependence of % DPPH inhibition and concentration of substances was investigated. The extract concentrations scavenged 50% of DPPH radicals were calculated by linear regression.

α-Glucosidase inhibitory assay Inhibitory activity on *α*-glucosidase was measured using fractionated extracts obtained from *Distichochlamys citrea* rhizomes according to the slightly modified method (Abdullah et al. 2016). The experimental design was described as follows: In 96-well plates, the reaction mixture consisted of 60 μl of test samples solution (concentration of 18.5 – 1125 μg/mL), 50 μl of 0.1 M phosphate buffer (pH 6.8) containing the enzyme *α*-glucosidase (0.2 U/mL) were incubated at 37 °C for 10 min. After pre-incubation, 50 μL of 5 mM *p*-nitrophenyl-*α*-D-glucopyranoside (*p*-NPG) solution in the above buffer was added. This mixture was further incubated at 37 °C for 20 min. The absorbance of the yields was measured at 405 nm using a microplate reader (Biotek, USA). Acarbose was used as a positive control.

The *α*-glucosidase inhibition rate expressed as a percentage of inhibition was calculated using the following formula:

$$\text{Inhibition of } \alpha - \text{glucosidase activity (\%)} = 1 - \frac{\left(A_c - A_{oc}\right) - \left(A_t - A_{ot}\right)}{\left(A_c - A_{oc}\right)} \times 100$$

where: A_c is the absorbance of the control (with enzyme without test extract). A_{oc} is the absorbance of the sample without enzyme and tested extract. A_t is the absorbance of the test sample (with enzyme and test extract). A_{ot} is the absorbance of the sample with test extract without enzyme.

The sample's capability to inhibit the enzyme *α*-glucosidase was based on the IC_{50} values (μg mL^{-1}); in essence, the concentration of the sample that results in 50% inhibition of maximal activity was determined.

Statistical analysis All experiments were in triplicate. All results were presented as mean values ± SD (Standard Deviation). The data results were calculated, analyzed, and graphically plotted using Microsoft Excel 2016. All statistical analyses were conducted under the analysis of variance (ANOVA) test. Statistical deviations were considered significant if the *p*-value was less than 0.05 ($p < 0.05$).

Computation

Quantum chemical calculation

Molecular quantum properties and their optimized geometry were retrieved by density functional theory (DFT) at the level of theory M052X/6–311 + + G(d,p) (Marković et al. 2011), using Gaussian 09 without symmetry constraints (Frisch et al. 2009). Calculations of vibrational frequencies were used to confirm the structural global minimum on the potential energy surface (PES). The basis set def2-TZVPP (Weigend and Ahlrichs 2005) was used to yield single-point energies at the M052X/6–311 + + G(d,p)-level-optimized geometries, resulting in the frozen-core approximation for non-valence-shell electrons. Each optimization run followed the resolution-of-identity (RI) approximation. NBO 5.1 was utilized to converge the frontier orbital analysis at the level of theory M052X/def2-TZVPP (Reed et al. 1985). The highest occupied molecular orbital (HOMO) energy, E_{HOMO}, represents intermolecular electron donation tendency; meanwhile, the electron-accepting ability of a molecule can be inferred from its value E_{LUMO} (for lowest unoccupied molecular orbital—LUMO). By exhibiting molecular electronic excitability, energy gap $\Delta E = E_{LUMO} - E_{HOMO}$ can suggest intermolecular reactivity of the host molecule. Koopman's theorem (Koopmans 1934) was applied on the frontier molecular orbital, giving ionization potential (I) and electron affinity (A): $I = -E_{HOMO}$ and $A = -E_{LUMO}$. The figures are useful indicators for the assessment of electronegativity (χ), hardness (η), softness (S), and other frontiers molecular orbital parameters, which in turn are useful in assessing the reactivity of a molecule. The molecule electronegativity (χ) can be determined by the equation: $\chi = (I + A)/2$; the hardness (η) can be expressed by $\eta = (I - A)/2$ and that of the softness is $S = 1/\eta$.

Molecular docking simulation

In a typical procedure, molecular docking simulation (by MOE 2015.10) follows four steps (Tarasova et al. 2018;

Thai et al. 2015; Ngo et al. 2016), yielding predictions on ligand–protein interactability.

Step 1 Pre-docking preparation

- Sources for simulation input: Crystal structure of protein P53341 (Fig. 2) of alpha-glucosidase from *Saccharomyces cerevisiae* was referenced from UniProtKB-P53341 (MAL12_YEAST) (https://www.uniprot.org/uniprot/P53341; February 22, 2022); Chemical formulae of ligands (Fig. 3) were from experimental findings by GC–MS in this work.

- Determination of protein active areas: Active amino acids were defined radius of 4.5 Å to ligands. Water or small molecules often detected by original experiments were removed; Configuration: Tether – Receptor with the strength of 5000; Refine of 0.0001 kcal•mol^{-1}•Å^{-1}. The output was saved in *.pdb format.

- Optimization of ligand energy minima: Ligand structures were geometrically optimized to check structural abnormality (if any); Configuration: Conj Grad for minima energy; termination for energy change = 0.0001 kcal·mol^{-1}; max interactions = 1000; modify charge: Gasteiger-Huckel.

Step 2 Docking investigation

- Configuration for docking simulation: poses retaining for intermolecular interaction probing = 10; maximum solutions per iteration = 1000; maximum solutions per fragmentation = 200. The obtained ligand–protein inhibitory structures were saved in format *.sdf.

Step 3 Re-docking iteration

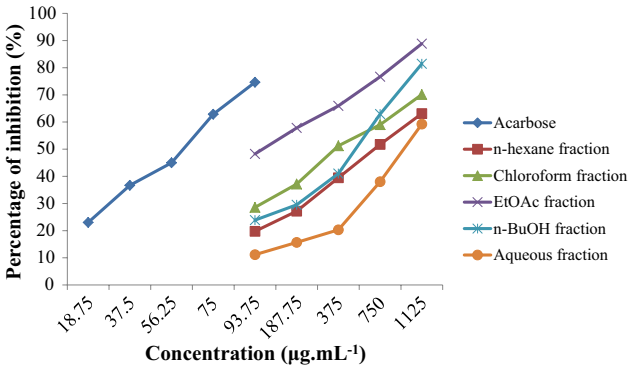

Fig. 3 In vitro α-glucosidase inhibitory activity of *Distichochlamys citrea* rhizomes fractionated extracts (percentage of inhibition (%) ± SD)

- Re-docking run was applied on the received protein-compound co-crystal structure for the purpose of checking the reliability of docking parameters.

Step 4 Post-docking analysis

- Docking score (DS) energy represents the Gibbs free energy of the respective ligand–protein inhibitory system, thus considered the primary indicator of inhibitory effectiveness. The value is contributed by attractive forces (hydrophilic binding and hydrophobic interaction) and geometrical complementarity (root-mean-square deviation—RMSD, i.e., the average between backbone atoms).

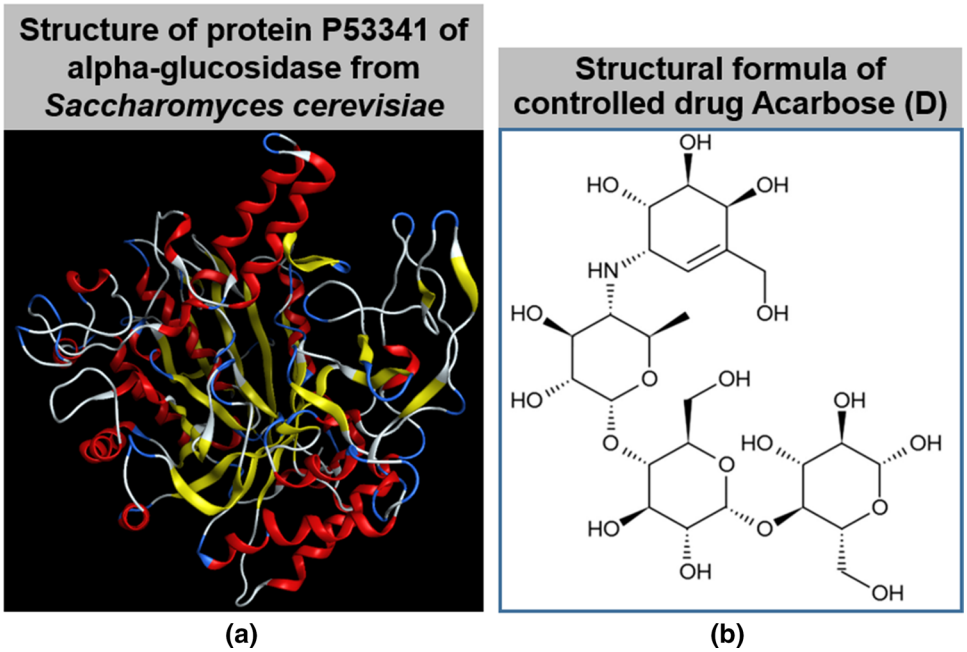

Fig. 2 Crystal structure of **a** protein P53341 of α-glucosidase from *Saccharomyces cerevisiae*. UniProtKB – P53341 (MAL12_YEAST) (https://www.uniprot.org/uniprot/P53341); and **b** structural formula of commercial medicine for diabetes treatment acarbose (**D**)

QSARIS-based analysis

Drug-likeness properties of the candidates were assessed by physicochemical properties given by the QSARIS system coupled with the reference from Lipinski's rule of five (Lipinski et al. 1997). The former is based on Gasteiger–Marsili method (Gasteiger and Marsili 1980), whose output parameters include molecular mass (Da), polarizability ($Å^3$) and volume or size (Å), and dispersion coefficients (logP and logS). The latter is a well-known set of criteria for assessment of orally pharmacological compatibility, described as (1) Molecular mass < 500 Da; (2) no more than 5 groups for hydrogen bonds; (3) no more than 10 groups receiving hydrogen bonds; (4) the value of logP is less than + 5 (logP < 5) (Ahsan et al. 2011; Mazumder et al. 2009).

ADMET-based analysis

A web environment developed and maintained by the Molecular Modeling Group, Swiss Institute of Bioinformatics, i.e., SwissADME (http://www.swissadme.ch/; February 22, 2022), was utilized to yield pharmacokinetic parameters including chemical absorption, distribution, metabolism, elimination and toxicity (ADMET) of the studied compounds. The theoretical interpretations of the parameters were described by Pires et al.(Pires et al. 2015) and powered by the University of Melbourne and University of Cambridge for public reference (http://biosig.unimelb.edu.au/pkcsm/theory).

Results and Discussion

Experimental

Pharmacognostic parameters

The average measurements of moisture content, total ash value, and acid-insoluble ash value of the rhizome powder are 12.41 ± 0.37 (%), 8.42 ± 0.26 (%), and 1.08 ± 0.08 (%), respectively. The sample achieved purity in terms of pharmacognostic parameters within the allowable limits of the Vietnamese Pharmacopoeia V for raw medicinal materials.

Phytochemical evaluation

The phytochemical screening of sample extracts of *Distichochlamys citrea* rhizome and leaf was performed. The results reveal the presence of essential oil, reduced sugars, amino acids, coumarins, and flavonoids in both rhizomes and leaves. Meanwhile, fats are found only in rhizomes but not in leaves. Otherwise, triterpenoids, carotenoids, saponins, cardiac glycosides, tannins, anthranoids, and polyuronides are not detected in both used parts.

The leaf sample was used for the preliminary phytochemical study to orientate further studies aiming to extend the medicinal parts of this herb.

Crude and fractionated extracts

Dried rhizomes powder 1.0 kg was under leaching with 96% ethanol (the ratio is 1:15) to obtain 103 g of total crude extract. The extraction yield of the crude extract is 10.3% with a moisture content of 12.0%. The weight, extraction yield and moisture content are determined for each fraction: *n*-hexane fraction (6.23 g, 6.05%, 14.0%), $CHCl_3$ fraction (42.0 g, 40.78%, 12.0%), EtOAc fraction (4.16 g, 4.04%, 15.0%), *n*-BuOH fraction (6.3 g, 6.12%, 17.2%), and aqueous fraction (26.8 g, 26.02%, 17.7%). To our knowledge, this is the first time the data is introduced to the literature.

The moisture content of the crude and fractionated extracts are within the allowable limit of the concentrated extract (not more than 20%) accordingly to the Vietnam Pharmacopoeia V.

Antioxidant activity by DPPH inhibition of fractionated extracts

Antioxidant activity of fractionated extracts of *Distichochlamys citrea* rhizome was determined based on DPPH free radical scavenging performance. The highest antioxidant activity is observed in the EtOAc fraction with the corresponding IC_{50} value of 90.27 μg mL^{-1}. In contrast, the other fractions perform the antioxidant activity of insignificance, given by the indeterminateness of IC_{50} values. Regarding the positive control (using ascorbic acid), the IC_{50} value registers 4.62 μg mL^{-1} (Eq.26, 25 μM; $p < 0.05$). The regression coefficients of both, aka. EtOAc fraction and ascorbic acid, are highly significant, i.e., $R^2 = 0.9925$ and 0.9936, respectively.

α-glucosidase inhibitory activity of fractionated extracts

The *α*-glucosidase inhibitory activity and the IC_{50} values of fractionated extracts are presented in Fig. 3 and Table 1, respectively. The EtOAc fraction exhibits a significant effect in inhibiting *α*-glucosidase, registering over 57% at concentration of 187.5 μg mL^{-1}, cf. others. Those

Table 1 IC_{50} values of the fractionated extracts of *Distichochlamys citrea* rhizomes and acarbose for inhibition of *α*-glucosidase

	Acarbose (p. control)	*n*-hexane fraction	$CHCl_3$ fraction	EtOAc fraction	*n*-BuOH fraction	Aqueous fraction
IC_{50} (μg mL^{-1})	58.51	621.37	371.37	115.75	545.98	965.70

of *n*-hexane, $CHCl_3$, *n*-BuOH, and aqueous fractions all record over 50% inhibition of α-glucosidase by concentrations of 750, 375, 750, and 1125 µg mL^{-1}, respectively. The α-glucosidase inhibitory activity of the fractionated extracts is concentration-dependent. The α-glucosidase inhibitory activity of the fractionated extracts follows the order: EtOAc fraction ($IC_{50} = 115.75$ µg mL^{-1}) > $CHCl_3$ fraction ($IC_{50} = 371.37$ µg mL^{-1}) > *n*-BuOH fraction ($IC_{50} = 545.98$ µg mL^{-1}) > *n*-hexane ($IC_{50} = 621.37$ µg mL^{-1}) > aqueous fraction ($IC_{50} = 965.70$ µg mL^{-1}). Also, the percentage inhibition of acarbose against α-glucosidase with IC_{50} values 58.51 µg mL^{-1} is given. The IC_{50} values of EtOAc, $CHCl_3$, *n*-BuOH, *n*-hexane, aqueous fractions, and acarbose (positive control) are of statistical significance $p < 0.05$. The regression coefficients of R^2 are 0.9860, 0.9862, 0.9981, 0.9807, 0.9885 and 0.9906, respectively. Given its promising bioactivity, more in-depth investigation on the EtOAc-faction chemical composition is highly justified.

Chemical composition of EtOAc extract

The chemical constituents of the EtOAc extract of *Distichochlamys citrea* rhizomes were determined by gas chromatography-mass spectrometry, summarized in Fig. 4 (structural formulae and denotations) and Table 2 (in-detail data). The EtOAc extract contains 13 chemical constituents and the major chemical constituents, including 5-Hydroxy methyl furfural (20.89%), 3-Deoxy-D-mannoic lactone (16.39%), 2,3-Dihydro-3,5-dihydroxy-6-methyl-4H-pyran-4-one (7.12%), monoacetin (6.77%), maltol (4.95%), γ-Decalactone (3.76%), propyl valerate (2.08%), 4-Chloroanisole (1.50%), 1-(3-Thiomorpholinyl)ethanone (1.49%), *p*-Meth-1-en-3,8-diol (1.49%), and vanillic acid (1.21%). Some other compounds are also detected in small quantity, i.e., methyl-6-oxoheptanoate (0.38%), and 1,3,3-trimethyl-2-oxabicyclo[2.2.2] octan-6-yl isobutyrate (0.72%). The findings can be subjected for further screenings on certain bioactive properties, either by experimental or computational approaches.

Discussion

In summary, the phytochemical screening of *Distichochlamys citrea* extracts reveals the presence of essential oil, flavonoids, coumarins, reducing compounds, fats, and amino acids. These phytochemicals are likely to contribute to various medicinal uses as well as nutritional supplementations of the herbs. Hithermost, only the plant family *Distichochlamys benenica* has been reported for the acetylcholinesterase inhibitory effect of its rhizome essential oil (Hoang et al. 2020) and the anti-inflammatory and antibacterial activities of its isolated compounds (Pham et al. 2021). Further than that, this work is the first time the biological effects of *Distichochlamys citrea* are reported in the literature.

Ascorbic acid is considered to be one of the most powerful, yet least toxic natural antioxidants. As a scavenger of ROS, ascorbic acid has been shown to be effective against the $O_2^{\cdot -}$, H_2O_2, $OH^{\cdot}$, $^1O_2$, and reactive $NO_2^{\cdot}$ (Gulcin 2020). The antioxidant capacity of the EtOAc fraction was found with IC_{50} values of 90.27 µg mL^{-1} and lower than ascorbic acid ($IC_{50} = 4.62$ µg mL^{-1}), ca. 19-fold. Nevertheless, the EtOAc fraction still exhibits the highest antioxidant capacity,

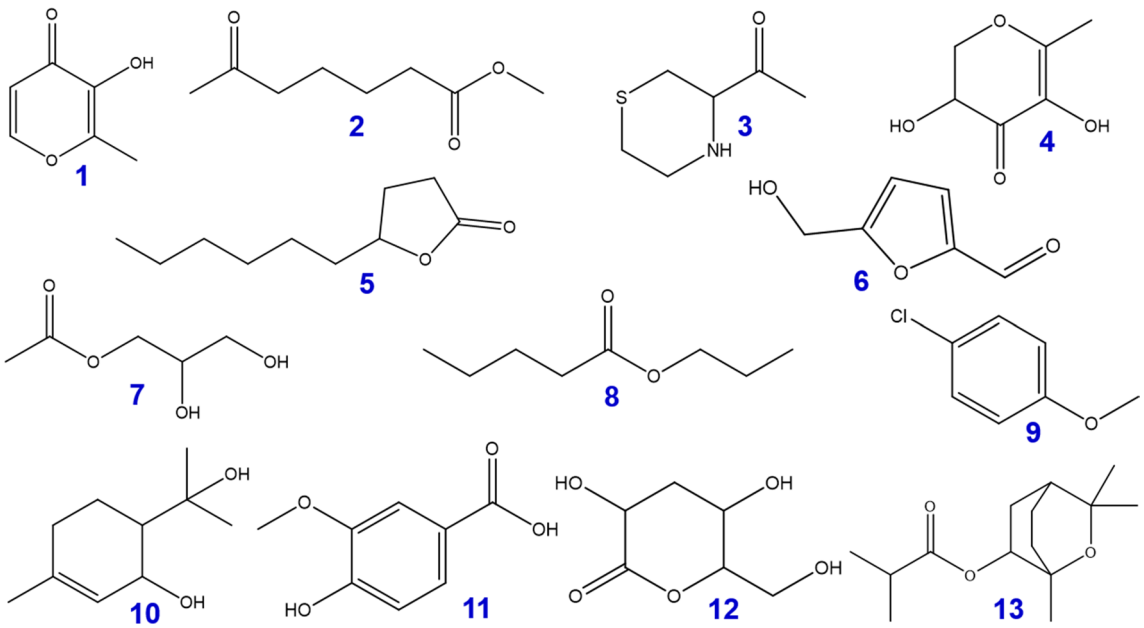

Fig. 4 Structural formula of compounds (**1–13**) from *Distichochlamys citrea* M.F. Newman rhizomes from the EtOAc extract

Table 2 Identification of major volatile bioactive compounds in EtOAc fraction of *Distichochlamys citrea* rhizomes

No	Retention time (min)	Substance	Formula	Symbol	Percentage (%)
1	3.64	Maltol	$C_6H_6O_3$	1	4.95
2	3.77	Methyl 6-oxoheptanoate	$C_8H_{14}O_3$	2	0.38
3	4.14	1-(3-Thiomorpholinyl)ethanone	$C_6H_{11}NOS$	3	1.49
4	4.25	2,3-Dihydro-3,5-dihydroxy-6-methyl-4H-pyran-4-one	$C_6H_8O_4$	4	7.12
5	4.70	γ-Decalactone	$C_{10}H_{18}O_2$	5	3.76
6	4.83	5-Hydroxy methyl furfural	$C_6H_6O_3$	6	20.89
7	4.95	Monoacetin	$C_5H_{10}O_4$	7	6.77
8	5.68	Propyl valerate	$C_8H_{16}O_2$	8	2.08
9	6.11	4-Chloroanisole	C_7H_7ClO	9	1.50
10	6.90	*p*-Meth-1-en-3,8-diol	$C_{10}H_{18}O_2$	10	1.49
11	7.08	Vanillic acid	$C_8H_8O_4$	11	1.21
12	7.48	3-Deoxy-D-mannoic lactone	$C_6H_{10}O_5$	12	16.39
13	11.48	1,3,3-Trimethyl-2-oxabicyclo[2.2.2]octan-6-yl isobutyrate	$C_{14}H_{24}O_3$	13	0.72

cf. other fractionated extracts. The up-bound capacity of the EtOAc fraction may be due to the presence of a higher quantity of flavonoids and other major volatile bioactive compounds. In extended studies, the compounds (i.e., flavonoids, coumarins, and essential oil) were reported to possess positive effects on human health, e.g., antibacterial, antioxidant, anti-diabetes, anti-inflammatory, and anti-allergic activities (Bouchelaghem et al. 2022; Xiao 2022; Gulcin et al. 2022). Oxidative stress resulting in the formation of free radicals was proved as a major factor in disease development and complications of diabetes (Tripathi and Chandra 2009). Our findings in this study indicate that all the fractionated extracts exhibit lower inhibition α-glucosidase in comparison to that of acarbose (IC_{50} 58.51 µg mL^{-1}). Particularly, the EtOAc fraction also registers a highly significant figure, i.e., IC_{50} value of 115.75 µg mL^{-1}, ca. 2 times lower than acarbose. The lowest is the aqueous fraction.

GC–MS-based metabolomics was used for the identification of the promising α-glucosidase inhibitors from the EtOAc fraction of *Distichochlamys citrea* rhizomes. The identified major compounds possess some important biological, promising for further studies on developing supplements or new drugs. The 5-Hydroxymethyl-2-furfural (20.89%) is a six-carbon heterocyclic aldehyde, containing alcohol and aldehyde functional groups (Kowalski et al. 2013). In preceding studies, 5-hydroxy methyl furfural compound was demonstrated to have an antioxidant, anti-allergic, anti-carcinogenic, anti-hypoxic, anti-apoptotic, anti-sickling agent, anti-inflammatory, anti-microbial, anti-hyperuricemic effects, and other activities (Zhao et al. 2013; Choudhary et al. 2021). The cyclic ester, 3-Deoxy-D-mannoic lactone (16.39%) is predominantly followed by alcoholic compounds. The compound, 3-Deoxy-D-mannoic lactone was reported for its antibacterial activity (Shobana et al. 2009). The 2,3-Dihydro-3,5-dihydroxy-6-methyl-4H-pyran-4-one (7.12%) is also found as one of the major compositions, reported for effective inhibition of colon cancer cell growth (Ban et al. 2007) and antioxidant activity (Chen et al. 2021). In addition, vanillic acid (4-hydroxy-3-methoxy benzoic acid) is a phenolic derivative from plants known to possess anti-filarial, antibacterial, antioxidant, and anti-diabetic (Vinothiya and Ashokkumar 2017; Wang et al. 2022), etc. Previous studies demonstrated maltol's effectiveness against oxidative damage (Song et al. 2015). It is able to prevent kidney damage in diabetic nephropathy (Kang et al. 2008), and diabetic peripheral neuropathy (Guo et al. 2018). In addition, maltol may be an efficient hepatoprotective agent (Sha et al. 2019) and slow age-associated brain aging (Rehder 2020). In recent years, rather simple coordination compounds such as maltol with iron supplements and VO $(maltol)_2$ (Vanadium) are now frequently used for the treatment of antidiabetics (Sagaama et al. 2020). It is noteworthy that GC–MS was specified in this work for the characterization of high-volatile components, which are commonly known as the main contributors to the enzymatic inhibitability of natural essential oils. On the other side, components with low-to-non volatility also hold untouched potentiality as *Distichochlamys citrea* M.F. Newman is an endemic plant, thus deserving further in-depth and in-scale investigations.

Despite their promising bioactive potent, it is still cost-inefficient and time-consuming to carry out experimental specifications, both high-grade purification and in vitro assaying, on all the compounds. Therefore, *in silico* screenings were opted in this stage, including quantum chemical examination (DFT-based), inhibitory probing (docking-based), physicochemical prediction (QSARIS-based), and regression for toxicity (ADMET-based).

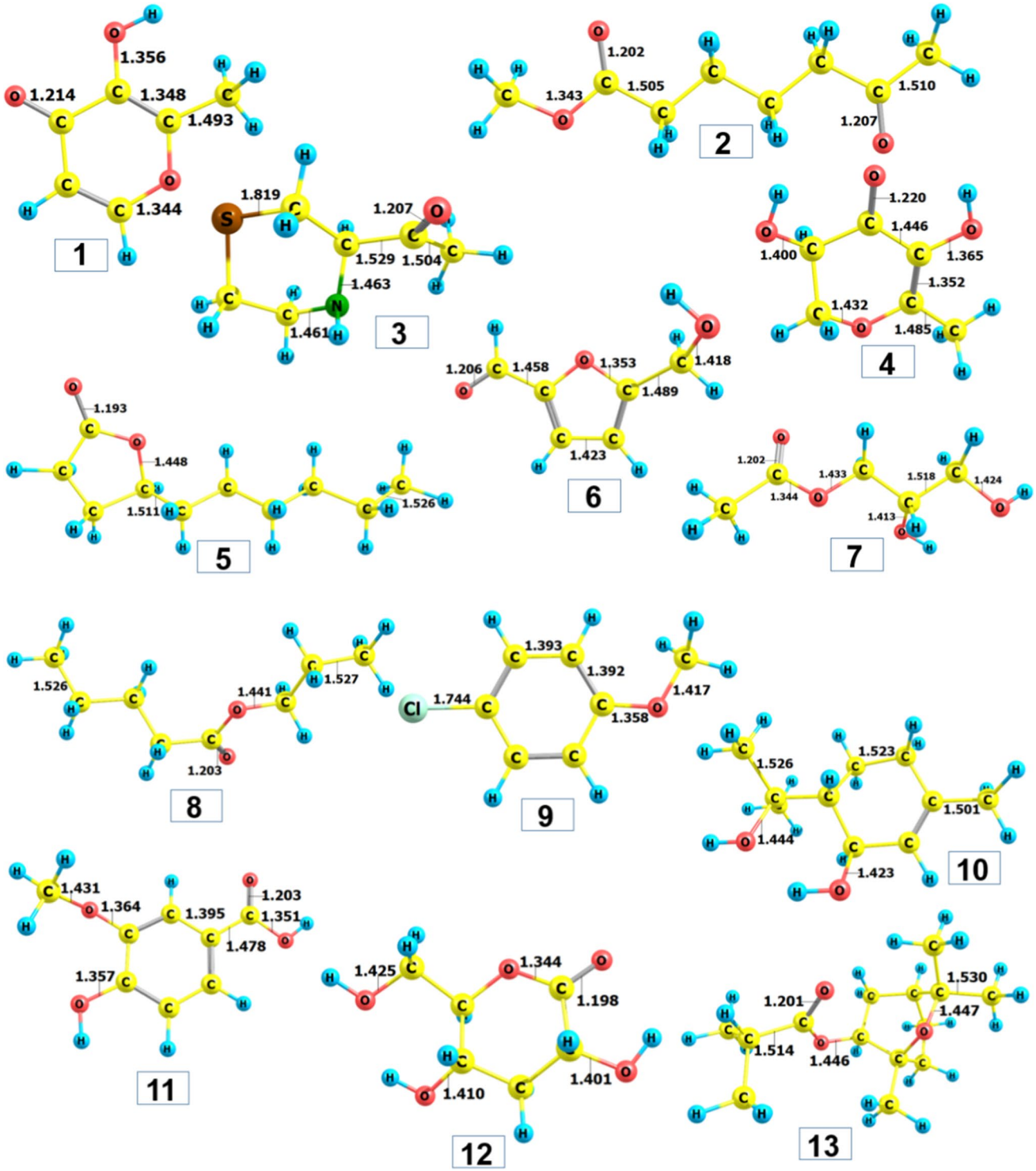

Fig. 5 Optimized structures of **1–13** calculated by DFT at level of theory M052X/6 − 311 + + g(d,p)

Computational

DFT-based optimized structures and quantum chemical properties

Density functional theory was utilised to re-check the natural formation of the bioactive compounds (**1–13**) and infer their intermolecular interactability, thus predicting their inhibitory capability.

Table 3 Ground state electronic energy and dipole moment values of **1–13** calculated by DFT at level of theory M052X/6–311 + + g(d,p)

Compound	Ground state electronic energy (kcal.mol^{-1})	Dipole moment (Debye)
1	− 287,374.86	5.860
2	− 338,257.58	1.470
3	− 479,091.78	2.698
4	− 335,356.08	2.053
5	− 340,393.37	4.926
6	− 287,371.10	2.741
7	− 312,259.33	2.712
8	− 291,802.71	2.271
9	− 506,038.59	2.812
10	− 340,380.24	3.965
11	− 383,201.53	4.064
12	− 383,333.31	4.966
13	− 462,945.50	2.817

Figure 5 presents the optimized structures in the ground state using the level of theory M052X/6–311 + + g(d,p); the corresponding ground state electronic energy and dipole moment values are retrieved in Table 3. Overall, structural convergence can be easily reached regarding all the compounds. This equals their in-nature stability, i.e., existence in natural sources. No abnormal bonding constraints, either angles or lengths are detected. All the calculated figures for the latter are in their characteristic values, e.g., 1.54 Å for C–C, 1.09 Å for C-H, 1.43 Å for C-O (oxatriquinane), 1.23 Å for C = O (carbonyl compounds), 1.74 Å for C–Cl, 1.47 Å for C-N, and 1.82 Å for C-S. The corresponding ground state electronic energies vary from -506,038.59 (**9**) to − 287,371.10 (**6**) kcal.mol^{-1}; and, those for the dipole moment are from 1.470 (**2**) to 5.860 (**1**) Debye. In principle, higher dipole moment values might correlate to the conduciveness to the formation of a bond or complex between the ligand and the target protein (Rad et al. 2021; Loan et al. 2020).

The highest occupied molecular orbital (HOMO) and lowest unoccupied molecular orbital (LUMO) of the optimized structures (**1–13**) are shown in Fig. 6; their in-detail quantum chemical parameters are retrieved in Table 4. Overall, different structures see different spatial localization of electron densities. Some distribute rather evenly over their molecular plane, e.g., **1**, **4**, **6**, **11**, and **12**, others localize the density into certain regions of their molecular structure. In theory, the former means the host molecules are more flexible for intermolecular interaction in terms of charge-transferring. This argument is based on the theoretical charge-transferring properties of HOMO (representing intermolecular electron donation tendency) and LUMO (representing electron-accepting ability). However, predominant stability is not highly justified since the property also depends on ligand-target chemical/physical affinity. Considering in-detail parameters, all structures (**1–13**) are considered exhibiting electronic stability of very high significance given low E_{HOMO}, which are all under − 7 eV (while commonly agreed under − 5 eV), especially **5** (− 9.450 eV), **7** (− 9.636 eV), **8** (− 9.428 eV), and **12** (− 9.660 eV). In another work of ours, theoretical complexes of a tetrylone family with the corresponding figures ranging from − 3 to − 7 eV were accepted as highly stable (Suresh 2010). Also, lying on the transition of an insulator (> 9 eV) and a semiconductor (< 3.2 eV) (Rosenberg 1962), the band-gap energy ΔE_{GAP} (between 6.446 and 8.880 eV) can be interpreted as conduciveness to intermolecular binding capability toward protein structures since the conductivity of the polypeptide molecules was well-observed and explained based on super-exchange theory (or electron tunneling) (Kharkyanen et al. 1978; Cordes and Giese 2009) and the electron hopping model (Thao et al. 2021a). Furthermore, their ionization potentials (aka. the opposite of ΔE_{HOMO}) of significance signify the difficulty of electron donation, thus preliminarily implying the tendency of intermolecular binding (via hydrophilic and hydrophobic bonds) over compositional changing (by chemical reactions).

Docking-based inhibitability

In the attempts to the prediction of ligand–protein inhibitability by in silico screening, *Distichochlamys citrea* compositional structures (**1–13**) and α-glucosidase crystal structure (**UniProtKB—P53341**) were selected for molecular docking simulation.

Figure 7 presents the quaternary structures of the targeted proteins, aka. *Saccharomyces cerevisiae* α-glucosidase MAL12, and its most susceptible sites to the ligands, aka. **1–13**. The main screening data are summarized in Table 5. The four most inhibition-effective sites are shaded in gray (site 1), yellow (site 2), blue (site 3), and cyan (site 4). It can be seen that although the protein structure is likely to be more vulnerable to the ligands at sites **1–3**, given higher total docking score (DS) values and number of hydrogen bonds, there is no explicitly consistent pattern across the inhibitors. Therefore, only the ligand–protein complexes regarding the most possibilities for an effective inhibition are selected for more in-depth discussion, which is signified in bold.

The selected data is summarized in Table 6; while, the corresponding visual projections (3D in-pose morphology and 2D interaction map) are presented in Fig. 8. Given the theoretical base of molecular docking simulation, DS values represent the average Gibbs free energy given by the contribution of ligand–protein attractive forces and the constrained distortion of ligand structures in order to shape into in-pose topographical features; and RMSD values are the average between neighboring backbone atoms, thus, in certain degrees, can be interpreted as bio-conformational rigidity or ligand–protein fitting. Accordingly, the most effective (DS < − 10 kcal.mol^{-1}) ligand–protein inhibitory structures might be in the order: **3-P53341** (DS -13.6 kcal.

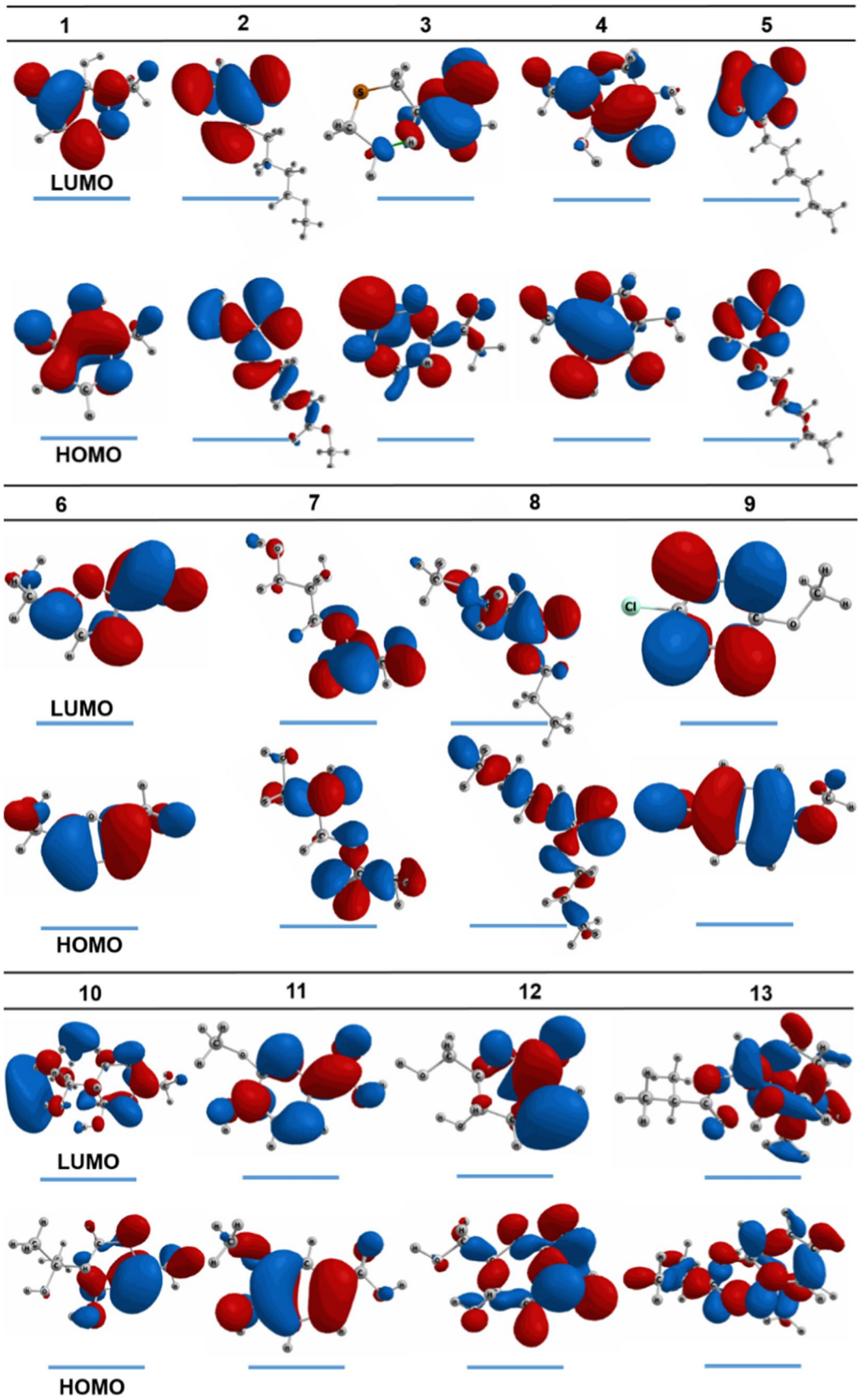

Fig. 6 HOMO and LUMO of **1–13** calculated by DFT at level of theory M052X/def2-TZV

Table 4 Quantum chemical parameters of compounds **1–13** calculated by NBO at the level of theory M052X/def2-TZVPP

Compound	E_{HOMO} (eV)	E_{LUMO} (eV)	ΔE_{GAP}	$I=-E_{HOMO}$	$A=-E_{LUMO}$	χ	μ	η	$S=1/\eta$
1	−8.030	−0.231	7.799	8.030	0.231	4.131	−4.131	3.8995	0.256
2	−8.868	−0.841	8.027	8.868	0.841	4.855	−4.855	4.0135	0.249
3	−7.511	−0.577	6.934	7.511	0.577	4.044	−4.044	3.467	0.288
4	−7.856	−0.702	7.154	7.856	0.702	4.279	−4.279	3.577	0.280
5	−9.450	−1.474	7.976	9.450	1.474	5.462	−5.462	3.988	0.251
6	−8.419	−0.977	7.442	8.419	0.977	4.698	−4.698	3.721	0.269
7	−9.636	−1.624	8.012	9.636	1.624	5.630	−5.630	4.006	0.250
8	−9.428	−1.591	7.837	9.428	1.591	5.510	−5.510	3.9185	0.255
9	−7.635	−0.304	7.331	7.635	0.304	3.970	−3.970	3.6655	0.273
10	−7.921	−1.475	6.446	7.921	1.475	4.698	−4.698	3.223	0.310
11	−8.079	−0.345	7.734	8.079	0.345	4.212	−4.212	3.867	0.259
12	−9.660	−0.780	8.880	9.660	0.780	5.220	−5.220	4.440	0.225
13	−8.296	−1.608	6.688	8.296	1.608	4.952	−4.952	3.344	0.299

Energy gap ($\Delta E_{GAP}=E_{LUMO}-E_{HOMO}$); Ionisation potential $I=-E_{HOMO}$
Electron affinity $A=-E_{LUMO}$; Electronegativity $\chi=(I+A)/2$
Chemical potential $\mu=-\chi=-(\partial E/\partial N)_{\nu(r)}$
Hardness $\eta=(I-A)/2$; Softness $S=1/\eta$

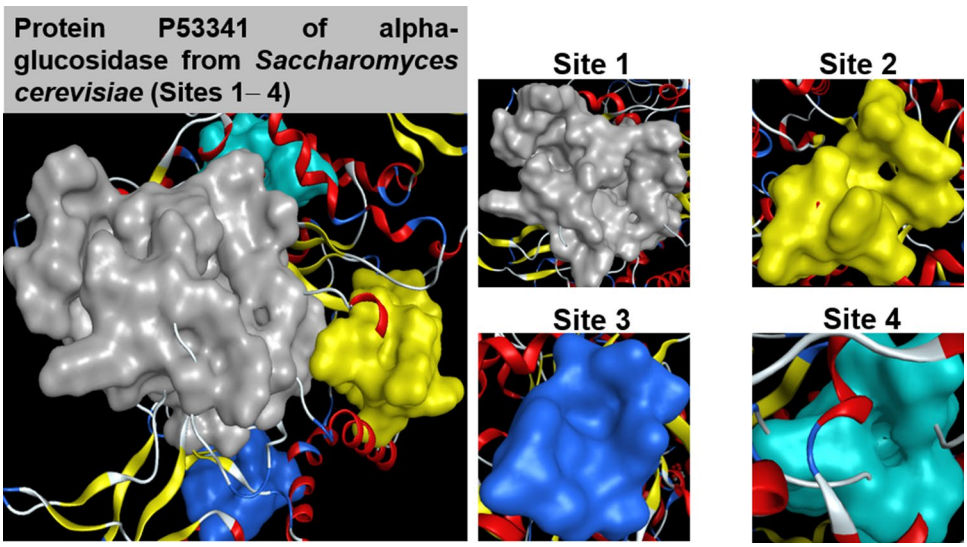

Fig. 7 Quaternary structures of protein P53341 with the approachable sites by **1–13** and the controlled drug Acarbose (**D**): site 1 (gray), site 2 (yellow), site 3 (blue), site 4 (cyan)

mol^{-1}; RMSD 1.31 Å) > **12-P53341** (DS -12.8 kcal.mol^{-1}; RMSD 0.94 Å) > **7-P53341** (DS -12.6 kcal.mol^{-1}; RMSD 0.59 Å) > **4-P53341** (DS -11.3 kcal.mol^{-1}; RMSD 0.88 Å) > **11-P53341** (DS -10.4 kcal.mol^{-1}; RMSD 1.41 Å) > **10-P53341** (DS -10.1 kcal.mol^{-1}; RMSD 1.45 Å). The corresponding figures for acarbose (**D**) are − 12.5 kcal.mol^{-1} and 1.07 Å. This preliminarily specifies **3** (i.e., structure of 1-(3-Thiomorpholinyl)ethanone) and **7** (i.e., structure of Monoacetin) as the most promising inhibitors against α-glucosidase; yet, the synergic effects of other components are still unknown. In other works of ours on the inhibitory effect of semi-synthesized derivatives from *Dolichandrone spathacea* iridoids and *Dipterocarpus alatus* dipterocarpol toward diabetes-related proteins, docking-based DS values at ca. − 13 to − 15 kcal.mol^{-1} correspond to assaying-based IC_{50} values < 10 µM (control drug IC_{50} ca. 300 µM) (Thao et al. 2021b; Feynman et al. 1965). Therefore, these compounds, especially 1-(3-Thiomorpholinyl)ethanone (**3**) and Monoacetin (**7**) deserve further experimental attempts for analytical graded isolation, structural re-determination, and in vitro bioassaying.

Projections of 2D interaction map and 3D in-pose morphology also provide certain leads to the potentiality of further development of the ligands. First, high-continuous

Table 5 Prescreening results on inhibitability of **1–13** and **D** toward the sites of protein P53341

P	L	Site 1		Site 2		Site 3		Site 4	
		E	N	E	N	E	N	E	N
P53341	1	−8.0	1	−7.2	1	**−9.0**	**2**	−6.5	0
	2	−8.4	1	**−9.4**	**2**	−6.8	0	−5.9	0
	3	**−13.6**	**7**	−10.6	4	−9.2	3	−9.7	3
	4	−9.0	2	**−11.3**	**4**	−7.5	1	−8.5	2
	5	−7.9	1	−8.3	1	**−9.2**	**2**	−6.6	0
	6	−8.3	1	**−10.8**	**3**	−7.1	0	−6.1	1
	7	**−12.6**	**5**	−10.6	3	−9.2	2	−8.5	2
	8	−7.3	1	−6.5	0	**−8.3**	**1**	−6.0	0
	9	**−9.5**	**2**	−7.3	1	−6.4	0	−6.0	0
	10	**−10.1**	**3**	−7.3	1	−9.2	2	−7.0	1
	11	−9.0	2	−7.0	1	**−10.4**	**3**	−7.3	1
	12	**−12.8**	**5**	−10.9	3	−9.4	2	−9.1	2
	13	−6.6	0	−7.3	1	**−8.6**	**1**	−6.2	0
	D	**−12.5**	**4**	−10.9	3	−9.3	2	−7.9	1

P Protein; *L* Ligand; *E* DS value (kcal.mol.$^{-1}$); *N* Number of hydrophilic interactions

Bold: Sites with most effective inhibition

contours in the former indicate the complementarity of the ligands to the in-pose features of their targeted protein sites. This means they are already leading frameworks regarding topographical fitting. Second, the latter reveals that the sites are observable rather small and close, cf. the studied inhibitors (**1–13**). This means significant further functionalization/modification on these compounds is not justifiably favorable in terms of spatial capacity.

Physicochemical properties

Table 7 summarizes QSARIS-based physicochemical properties of the investigated compounds (**1–13** and **D**), which are molecular mass (amu), polarisability (Å^3) and size (Å) as well as the logP and logS dispersion coefficients. Since molecular docking simulation begins based on the assumption that the ligands are already placed in an interactable radius to the protein (aka. 4.5 Å in this work), there is no retrieval for their pre-docking biocompatibility. Hence, their physicochemical properties coupled with Lipinski's drug-like criteria are utilized to retrieve an overview of potential ligand-plasma interaction in the polarized media of biological bodies. Overall, all the candidates are in excellent satisfaction to Lipinski's requirements, i.e., molecular mass < 500 amu (max. 242.5 amu; **13**) and dispersion coefficients logP < + 5 (max. 2.46; **9**). Their hydrophilic behavior briefly referenced from docking-based retrievals are also likely to satisfy the criteria. The figures are counted from the number of hydrogen-bond types formed in inhibitory simulation. In addition, their polarisability constants are considerable, implicating the likelihood of inducing the formation of molecular dielectric moments (Feynman et al. 1965). In summary, from the view of physicochemical properties, all the studied candidates (**1–13**) are in essence biocompatible for drug-developing applications.

ADMET-based pharmacokinetics and pharmacology

Table 8 presents the chemical absorption, distribution, metabolism, excretion, and toxicity (ADMET) of the investigated compounds (**1–13** and **D**). The theoretical interpretations of the parameters were described by Pires et al.(Pires et al. 2015) and powered by The University of Melbourne and University of Cambridge for public reference (http://biosig.unimelb.edu.au/pkcsm/theory; February 22, 2022).

First, all the candidates (**1–13**) hold significant effectiveness of intestine absorbance by the percentage of over 70% (considerably high at > 30%), while that of **D** is only ca. 4%. Nevertheless, their corresponding values of logPaap for Caco2 permeability are rather low, under 2×10^{-6} cm. s^{-1}. This means although they can be absorbed effectively through the intestine, their overall intestinal processes, i.e., transcellular transport, paracellular transport, and some aspects of efflux-active transport, would meet certain resistance. Therefore, transport-enhanced synergic agents should be in consideration if in practice. The modeling also predicts almost no ligand-P-glycoprotein interactions, meaning no significant interruption to transmembrane activities. Second, the composition in total tends to accumulate in tissue (given low values of log VDss) rather than be carried out in plasma. Except for 5, 8, and 9, they also seem unable to cross

Table 6 Molecular docking simulation results for ligand – P53341 inhibitory complexes

Ligand – protein complex			Hydrogen bond						van der Waals interaction
Name	DS	RMSD	L	P		T	D	E	
1-P53341	−9.0	0.68	O	O	Glu 77	H-donor	3.03	−2.4	His 116, Glu 117, Ser 198, Asn 75
			O	N	Trp 118	H-acceptor	2.97	−1.7	
2-P53341	−9.4	1.61	O	N	Ser 295	H-acceptor	2.94	−2.0	Lys 262, Glu 270. Met 261, His 258. Tyr 292. Val 294, Trp 14, Glu 293, Ala 289
			O	N	Ile 271	H-acceptor	3.18	−1.2	
3-P53341	−13.6	1.31	C	O	Asp 349	H-donor	3.60	−0.7	His 111, Arg 439. Phe 177, Phe 158, Glu 276, Arg 212, Thr 215
			C	O	Asp 349	H-donor	3.09	−0.8	
			S	O	Asp 68	H-donor	3.08	−1.5	
			S	N	Gln 181	H-acceptor	3.77	−2.0	
			N	O	Asp 214	Ionic	3.54	−1.7	
			N	O	Sap 349	Ionic	3.12	−3.7	
			C	6 – ring	Tyr 71	H-pi	4.37	−0.9	
4-P53341	−11.3	0.88	O	O	Ala 289	H-donor	3.39	−0.8	Tyr 292, His 258, Val 294, Met 272, Trp 14
			O	O	Ile 271	H-donor	3.0	−1.0	
			C	O	Glu 270	H-donor	3.5	−0.8	
			O	O	Ser 295	H-acceptor	2.96	−1.5	
5-P53341	−9.2	1.70	O	N	Tyr 76	H-acceptor	3.15	−2.7	Asn 75, Glu 77. Trp 118, Ser 198, Ala 194, Glu 197
			O	N	His 116	H-acceptor	2.93	−1.2	
6-P53341	−10.8	1.78	O	O	Ile 271	H-donor	2.83	−1.9	His 258, Val 294, Lys 12, Trp 14, Glu 270, Met 272. Glu 293
			O	O	Thr 273	H-acceptor	2.92	−1.3	
			5 – ring	O	Ser 295	π – H	3.36	−0.7	
7-P53341	−12.6	0.59	C	O	Asp 349	H-donor	3.45	−0.6	Phe 158, His 111, Thr 215, Tyr 71, Glu 276, Arg 439, Phe 157, Phe 177
			O	O	Asp 214	H-donor	3.07	−2.9	
			O	O	Asp 349	H-donor	3.00	−1.8	
			O	N	Arg 212	H-acceptor	3.26	−0.6	
			O	N	His 348	H-acceptor	3.13	−0.9	
8-P53341	−8.3	1.62	O	N	Trp 118	H-acceptor	3.13	−1.0	Glu 197, Ala 194, Asn 75, Ser 74, Glu 77, Glu 117, His 116, Ser 198
9-P53341	−9.5	1.29	C	6 – ring	Tyr 71	H-pi	3.77	−0.6	Arg 439, Phe 300, Phe 157, Thr 215, Asp 214, Glu 276, His 348, Asp 68, Asp 349, Phe 158, Arg 439, Phe 300
			6 – ring	C	Phe 177	π – H	3.78	−0.7	
10-P53341	−10.1	1.45	O	O	Glu 276	H-donor	3.22	−0.8	Thr 215, Asp 214, His 348, Arg 439, Asp 68, Tyr 71, His 111, Gln 181, Phe 177, Phe 158, Phe 300
			O	O	Asp 349	H-donor	2.69	−2.1	
			O	N	Arg 212	H-acceptor	2.96	−2.8	
11-P53341	−10.4	1.41	O	O	Glu 77	H-donor	2.88	−1.9	Glu 117, His 116, Asn 75, Ser 198, Ser 74, Trp 118
			O	O	Glu 121	H-donor	3.18	−4.7	
			O	N	Lys 130	H-acceptor	3.25	−3.6	
12-P53341	−12.8	0.94	O	O	Asp 349	H-donor	3.02	−2.0	Asp 68, Tyr 71, Arg 443, Arg 439, Phe 158, Phe 177, Phe 300, Glu 276, Thr 215, Asp 214
			O	O	Asp 349	H-donor	3.24	−1.3	
			O	O	Asp 349	H-donor	2.93	−1.5	
			O	N	Arg 212	H-acceptor	2.84	−4.2	
			O	N	His 348	H-acceptor	3.00	−0.8	
13-P53341	−8.6	1.25	O	N	Asn 75	H-acceptor	3.06	−3.6	Glu 117, Trp 118, Glu 77, Ser 198, His 116
D-P53341	−12.5	1.07	O	N	Arg 312	H-acceptor	3.13	−0.7	Asp 408, Asp 349, Arg 439, Phe 158, Thr 307, Thr 215, Glu 304, Phe 157, Phe 300, Glu 276, Phe 177, Ser 308, Ala 278, Pro 309, His 279, Phe 310, Phe 213
			O	N	Asn 241	H-acceptor	2.88	−1.7	
			N	N	Arg 312	H-acceptor	3.45	−1.7	
			C	5 – ring	His 239	H-π	3.17	−0.6	

DS Docking score energy (kcal.mol^{-1}); *RMSD* Root – mean – square deviation (Å); *L* Ligand; *P* Protein; *T* Type; *D* Distance (Å); *E* Energy (kcal.mol.$^{-1}$)

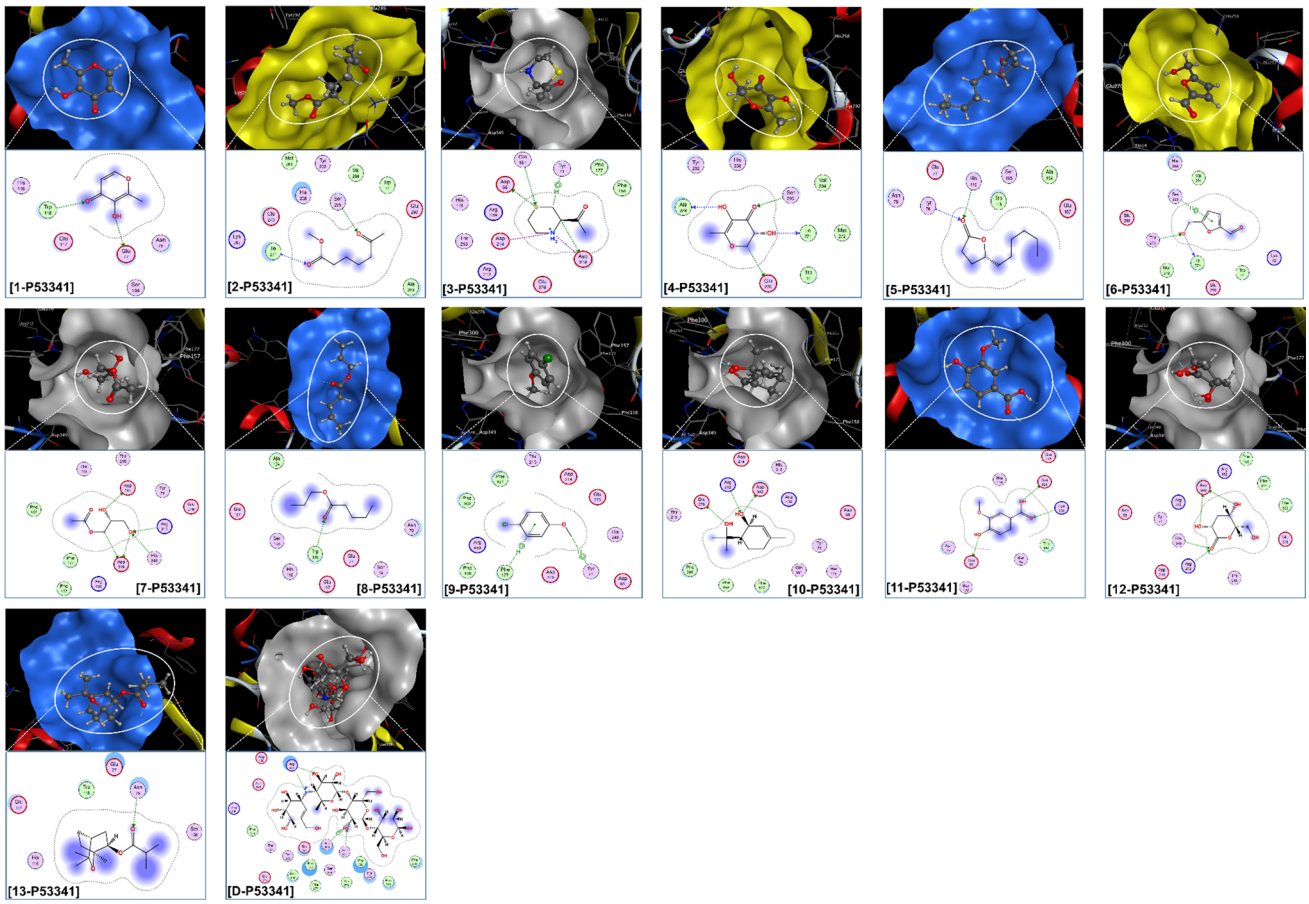

Fig. 8 Visual presentation and in – pose interaction map of and ligand – P53341 (**1–13** and **D**) inhibitory structures

Table 7 Physicochemical properties of studied compounds **1 – 13** and **D**

Compound	Mass	Polarisability	Size	Dispersion coefficients		Bonding site		
				LogP	LogS	Total bonding	H-acceptor	H-donor
1	127.0	14.3	156.8	0.92	− 1.62	2	1	1
2	158.9	17.1	268.7	0.75	− 1.08	.2	2	0
3	146.0	16.5	223.1	0.47	− 0.92	7	1	3
4	145.2	13.7	180.1	0.21	− 0.43	4	1	3
5	172.0	20.2	301.7	2.23	− 2.43	2	2	0
6	128.2	14.9	171.5	0.87	− 0.13	3	1	1
7	134.9	12.8	190.7	1.24	− 0.93	5	3	2
8	145.6	17.8	284.6	2.47	− 1.82	1	1	0
9	143.2	16.3	210.2	2.46	− 2.73	2	1	0
10	172.4	20.1	269.4	1.69	− 1.73	3	1	2
11	171.2	17.8	220.3	1.34	− 1.52	3	1	2
12	162.9	14.8	189.3	1.07	− 0.87	5	2	3
13	242.5	24.3	289.5	2.09	− 2.34	1	1	0
D	643.7	58.9	623.6	2.98	− 1.94	4	3	0

Table 8 ADMET – based pharmacokinetics and pharmacology of the studied compounds **1 – 13** and **D**

Property	1	2	3	4	5	6	7	8	9	10	11	12	13	D	Unit
	Absorption														
Water solubility	− 1.437	− 0.716	− 0.108	− 0.234	− 2.749	− 0.59	0.678	− 1.711	− 2.319	− 1.254	− 1.838	− 0.159	− 3.174	− 1.482	Numeric (log mol.L^{-1})
Caco2 permeability	1.178	1.221	1.466	0.574	1.6	1.172	0.61	1.418	1.539	1.58	0.33	0.568	1.712	− 0.481	Numeric (log Papp in 10^{-6} cm.s^{-1})
Intestinal absorption (human)	98.227	99.245	100	84.187	95.17	95.848	78.648	95.867	94.617	94.429	78.152	71.857	97.031	4.172	Numeric (% Absorbed)
Skin Permeability	− 3.085	− 2.363	− 3.565	− 3.615	− 1.937	− 3.416	− 4.255	− 2.004	− 1.723	− 3.602	− 2.726	− 3.71	− 2.932	− 2.735	Numeric (log Kp)
P-glycoprotein substrate	No	No	Yes	No	No	No	No	No	No	No	No	No	No	Yes	Categorical (Yes/No)
P-glycoprotein I inhibitor	No	No	No	No	No	No	No	No	No	No	No	No	No	No	Categorical (Yes/No)
P-glycoprotein II inhibitor	No	No	No	No	No	No	No	No	No	No	No	No	No	No	Categorical (Yes/No)
	Distribution														
VDss (human)	− 0.027	− 0.263	0.33	− 0.174	0.194	− 0.146	− 0.372	− 0.025	0.092	− 0.083	− 1.739	− 0.271	0.31	− 0.836	Numeric (log L.kg^{-1})
Fraction unbound (human)	0.73	0.589	0.833	0.781	0.461	0.744	0.837	0.549	0.346	0.639	0.518	0.885	0.425	0.505	Numeric (log L.kg^{-1})
BBB permeability	− 0.353	− 0.178	− 0.002	− 0.324	0.595	− 0.361	− 0.367	0.445	0.433	− 0.177	− 0.38	− 0.533	0.117	− 1.717	Numeric (log BB)
CNS permeability	− 2.883	− 2.463	− 3.068	− 3.391	− 2.385	− 2.914	− 3.452	− 2.371	− 1.837	− 3.059	− 2.628	− 3.551	− 2.906	− 6.438	Numeric (log PS)
	Metabolism														
CYP2D6 substrate	No	No	No	No	No	No	No	No	No	No	No	No	No	No	Categorical (Yes/No)
CYP3A4 substrate	No	No	No	No	No	No	No	No	No	No	No	No	No	No	Categorical (Yes/No)
CYP1A2 inhibitior	No	No	No	No	No	No	No	No	No	No	No	No	No	No	Categorical (Yes/No)
CYP2C19 inhibitior	No	No	No	No	No	No	No	No	No	No	No	No	No	No	Categorical (Yes/No)
CYP2C9 inhibitior	No	No	No	No	No	No	No	No	No	No	No	No	No	No	Categorical (Yes/No)
CYP2D6 inhibitior	No	No	No	No	No	No	No	No	No	No	No	No	No	No	Categorical (Yes/No)
CYP3A4 inhibitior	No	No	No	No	No	No	No	No	No	No	No	No	No	No	Categorical (Yes/No)
	Excretion														
Total Clearance	0.661	0.84	1.006	0.505	1.392	0.614	0.836	0.553	0.251	1.25	0.628	0.666	0.984	0.428	Numeric (log ml.min^{-1}.kg^{-1})
Renal OCT2 substrate	No	No	No	No	No	No	No	No	No	No	No	No	Yes	No	Categorical (Yes/No)
	Toxicity														
AMES toxicity	No	No	No	Yes	No	No	Yes	No	No	No	No	No	No	No	Categorical (Yes/No)
Max. tolerated dose (human)	0.466	0.811	0.57	1.22	0.503	0.77	1.537	0.832	1.102	1.134	0.719	1.421	0.274	0.435	Numeric (log mg.kg^{-1}.day^{-1})
hERG I inhibitor	No	No	No	No	No	No	No	No	No	No	No	No	No	No	Categorical (Yes/No)
hERG II inhibitor	No	No	No	No	No	No	No	No	No	No	No	No	No	Yes	Categorical (Yes/No)
Oral Rat Acute Toxicity (LD50)	2.162	1.978	2.339	1.852	1.866	2.283	1.534	1.937	2.215	1.654	2.454	1.409	2.041	2.449	Numeric (mol/kg)

Table 8 (continued)

Property	1	2	3	4	5	6	7	8	9	10	11	12	13	D	Unit
Oral Rat Chronic Toxicity (LOAEL)	1.839	2.538	0.865	2.671	2.297	2.488	2.783	2.351	1.957	2.529	2.032	2.428	1.847	5.319	Numeric (log mg.kg^{-1} _ bw.day^{-1})
Hepatotoxicity	No	No	No	No	No	No	No	No	No	No	No	No	No	No	Categorical (Yes/No)
Skin Sensitization	No	Yes	No	No	Yes	No	No	Yes	Yes	Yes	No	No	Yes	No	Categorical (Yes/No)
T.Pyriformis toxicity	−0.294	−0.204	−0.8	−0.209	0.327	−0.767	−0.381	0.104	0.461	−0.736	0.265	0.114	0.454	0.285	Numeric (log ug.L^{-1})
Minnow toxicity	2.644	1.73	2.645	2.488	0.897	2.836	3.366	1.192	1.195	2.143	1.926	3.402	1.221	16.823	Numeric (log mM)

the blood–brain barrier given their low BBB permeability (logBB < −1). The exception is of **4**, **7**, and **12** regarding the inability of the central nervous system given their low CNS permeability (logPS < −3). Third, no possible effects on the inhibitors and substrates relating to the cytochromes P450 family are regressed regarding any of the candidates; thereby, in general, they can be effectively oxidized in the liver. In terms of excretion, most of the candidates (except for **13**) are expected to be carried out of the body by Organic Cation Transporter 2, with the total clearance being ca. 0.2–1.5 log ml.min^{-1}.kg^{-1}. In terms of toxicity, most test compounds are considered as being safe. Only **4** and **7** express mutagenic potentials represented by AMES toxicity; No potential agents for fatal ventricular arrhythmia; No potential agents for hepatotoxicity. Therefore, this regression preliminarily encourages further investigations on the biological potentiality of *Distichochlamys citrea* compositional structures (**1–13**).

Conclusion

This study first-time demonstrates antioxidant and α-glucosidase inhibitory activities of fractionated extracts from *Distichochlamys citrea* rhizomes, an endemic plant species found only in Vietnam. The plant was under DNA-based identification and approved by GenBank under the code MZ310840.1. Antioxidant activity by DPPH inhibition of fractionated extracts registers only at EtOAc fraction with the corresponding IC_{50} value 90.27 µg mL^{-1}; α-glucosidase inhibitory activity of fractionated extracts registers into the order: EtOAc fraction (IC_{50} = 115.75 µg mL^{-1}) > $CHCl_3$ fraction (IC_{50} = 371.37 µg mL^{-1}) > n-BuOH fraction (IC_{50} = 545.98 µg mL^{-1}) > *n*-hexane (IC_{50} = 621.37 µg mL^{-1}) > aqueous fraction (IC_{50} = 965.70 µg mL^{-1}). The EtOAc extract contains 13 chemical constituents: 5-Hydroxy methyl furfural (20.89%), 3-Deoxy-D-mannoic lactone (16.39%), 2,3-Dihydro-3,5-dihydroxy-6-methyl-4H-pyran-4-one (7.12%), monoacetin (6.77%), maltol (4.95%), γ-Decalactone (3.76%), propyl valerate (2.08%), 4-Chloroanisole (1.50%), 1-(3-Thiomorpholinyl)ethanone (1.49%), *p*-Meth-1-en-3,8-diol (1.49%), vanillic acid (1.21%), methyl-6-oxoheptanoate (0.38%), and 1,3,3-trimethyl-2-oxabicyclo[2.2.2]octan-6-yl isobutyrate (0.72%). DFT-based calculations find no abnormal structural constraints of the compounds, thus supporting their natural existence. Docking-based essential order for most effective ligand–protein inhibitory structures is: **3-P53341** (DS -13.6 kcal.mol^{-1}; RMSD 1.31 Å) > **12-P53341** (DS -12.8 kcal.mol^{-1}; RMSD 0.94 Å) > **7-P53341** (DS -12.6 kcal.mol^{-1}; RMSD 0.59 Å) > **4-P53341** (DS -11.3 kcal.mol^{-1}; RMSD 0.88 Å) > **11-P53341** (DS -10.4 kcal.mol^{-1}; RMSD 1.41 Å) > **10-P53341** (DS -10.1 kcal.mol^{-1}; RMSD 1.45 Å).

QSARIS-based investigations implicate the biocompatibility of the candidates for drug developments. ADMET-based regressions especially suggest all the compounds are generally safe for medicinal applications. The results obtained in this work would encourage further experimental attempts for high-degree isolation, structural re-determination, and more in-depth bio-assaying on the most potential compounds.

Supplementary Information The online version contains supplementary material available at https://doi.org/10.1007/s11696-022-02273-2.

Acknowledgements This research was funded by the Ministry of Education and Training (Vietnam) for the development of Science and Technology, with code B2021-DHH-13. The authors thank the partial facility support of Faculty of Traditional Medicine, University of Medicine and Pharmacy at Ho Chi Minh City for testing in vitro antioxidants and α-glucosidase inhibitory activities.

Declarations

Conflict of interest On behalf of all authors, the corresponding author states that there is no conflict of interest.

References

Abdullah NH, Salim F, Ahmad R (2016) Chemical constituents of Malaysian *U cordata var ferruginea* and their in vitro α-glucosidase inhibitory activities. Molecules 21(5):525. https://doi.org/10.3390/molecules21050525

Ahsan MJ, Samy JG, Khalilullah H, Nomani MS, Saraswat P, Gaur R, Singh A (2011) Molecular properties prediction and synthesis of novel 1, 3, 4-oxadiazole analogues as potent antimicrobial and antitubercular agents. Bioorganic Med Chem Lett 21(24):7246–7250. https://doi.org/10.1016/j.bmcl.2011.10.057

Akmal M, Wadhwa R (2021) Alpha glucosidase inhibitors. StatPearls [Internet]. PMID: 32496728. https://www.ncbi.nlm.nih.gov/books/NBK557848/

Alam F, Islam MA, Kamal MA, Gan SH (2018) Updates on managing type 2 diabetes mellitus with natural products: towards antidiabetic drug development. Curr Med Chem 25(39):5395–5431. https://doi.org/10.2174/0929867323666160813222436

American Diabetes Association (2018) 2 Classification and diagnosis of diabetes: standards of medical care in diabetes–2018 Diabetes care 41(Supplement_1), S13-S27 https://doi.org/10.2337/dc18-S002

Ban JO, Hwang IG, Kim TM, Hwang BY, Lee US, Jeong HS, Hong JT (2007) Anti-proliferate and pro-apoptotic effects of 2, 3-dihydro-3, 5-dihydroxy-6-methyl-4H-pyranone through inactivation of NF-κB in human colon cancer cells. Arch Pharm Res 30(11):1455–1463. https://doi.org/10.1007/BF02977371

Blahova J, Martiniakova M, Babikova M, Kovacova V, Mondockova V, Omelka R (2021) Pharmaceutical drugs and natural therapeutic products for the treatment of type 2 diabetes mellitus. Pharmaceuticals 14(8):806. https://doi.org/10.3390/ph14080806

Bouchelaghem S, Das S, Naorem RS, Czuni L, Papp G, Kocsis M (2022) Evaluation of total phenolic and flavonoid contents, antibacterial and antibiofilm activities of *Hungarian Propolis* ethanolic extract against *Staphylococcus aureus*. Molecules 27(2):574. https://doi.org/10.3390/molecules27020574

C.I Methodology of Analysis of Vegetable and Drugs (1984) Rumania: Ministry of Chemical Industry, Bucharest

Chen Z, Liu Q, Zhao Z, Bai B, Sun Z, Cai L, Xi G (2021) Effect of hydroxyl on antioxidant properties of 2, 3-dihydro-3, 5-dihydroxy-6-methyl-4 H-pyran-4-one to scavenge free radicals. RSC Adv 11(55):34456–34461. https://doi.org/10.1039/D1RA06317K

Choudhary A, Kumar V, Kumar S, Majid I, Aggarwal P, Suri S (2021) 5-Hydroxymethylfurfural (HMF) formation, occurrence and potential health concerns: recent developments. Toxin Rev 40(4):545–561. https://doi.org/10.1080/15569543.2020.1756857

Cordes M, Giese B (2009) Electron transfer in peptides and proteins. Chem Soc Rev 38(4):892–901. https://doi.org/10.1039/b805743p

Costa-Latgé SGD, Bates P, Dillon RJ, Genta FA (2021) Characterization of glycoside hydrolase families 13 and 31 reveals expansion and diversification of α-amylase genes in the phlebotomine Lutzomyia longipalpis and modulation of sandfly glycosidase activities by Leishmania infection. Front Physiol 12:341. https://doi.org/10.3389/fphys.2021.635633

Del Moral S, Barradas-Dermitz DM, Aguilar-Uscanga MG (2018) Production and biochemical characterization of α-glucosidase from *Aspergillus niger* ITV-01 isolated from sugar cane bagasse. 3 Biotech 8(1):1–9. https://doi.org/10.1007/s13205-017-1029-6

DiNicolantonio JJ, Bhutani J, O'Keefe JH (2015) Acarbose: safe and effective for lowering postprandial hyperglycaemia and improving cardiovascular outcomes. Open Heart 2(1):e000327. https://doi.org/10.1136/openhrt-2015-000327

Draznin B, Aroda VR, Bakris G, Benson G, Brown FM, Freeman R, Kosiborod M (2022) 2. Classification and diagnosis of diabetes: standards of medical care in diabetes-2022. Diabetes Care 45(1):S17–S38. https://doi.org/10.2337/dc22-s002

Dušan V, Nenad M, Dejan B, Filip B, Segal AM, Dejan Š, Aleksandra D (2014) The specificity of α-glucosidase from *Saccharomyces cerevisiae* differs depending on the type of reaction: hydrolysis versus transglucosylation. Appl Microbiol Biotechnol 98(14):6317–6328. https://doi.org/10.1007/s00253-014-5587-9

Eberle C, Stichling S (2021) Impact of COVID-19 lockdown on glycemic control in patients with type 1 and type 2 diabetes mellitus: a systematic review. Diabetol Metab Syndr 13(1):1–8. https://doi.org/10.1186/s13098-021-00705-9

Ferreira LG, Dos Santos RN, Oliva G, Andricopulo AD (2015) Molecular docking and structure-based drug design strategies. Molecules 20(7):13384–13421. https://doi.org/10.3390/molecules200713384

Feynman RP, Leighton RB, Sands M (1965) The feynman lectures on physics; vol i. Amer J Phys 33(9):750–752. https://doi.org/10.1119/1.1972241

Frisch GWTMJ, Schlegel HB, Scuseria GE, Robb MA, Cheeseman JR, Scalmani G, Barone V, Mennucci B, Petersson GA, Nakatsuji H, Caricato M, Li X, Hratchian HP, Izmaylov AF, Bloino J, Zheng G, Sonnenberg JL, Hada M, Eh M, Fox DJ (2009) Gaussian 09. Gaussian Inc., Wallingford

Gasteiger J, Marsili M (1980) Iterative partial equalization of orbital electronegativity—a rapid access to atomic charges. Tetrahedron 36(22):3219–3228. https://doi.org/10.1016/0040-4020(80)80168-2

Gregory JM, Slaughter JC, Duffus SH, Smith TJ, LeStourgeon LM, Jaser SS, Moore DJ (2021) COVID-19 severity is tripled in the diabetes community: a prospective analysis of the pandemic's impact in type 1 and type 2 diabetes. Diabetes Care 44(2):526–532. https://doi.org/10.2337/dc20-2260

Gulcin İ (2020) Antioxidants and antioxidant methods: an updated overview. Arch Toxicol 94(3):651–715. https://doi.org/10.1007/s00204-020-02689-3

Gulcin I, Bingöl Z, Taslimi P, Gören AC, Alwasel SH, Tel AZ (2022) Polyphenol contents potential antioxidant anticholinergic and antidiabetic properties of mountain mint (Cyclotrichium

leucotrichum). Chem Biodivers. https://doi.org/10.1002/cbdv.202100775
Guo N, Li C, Liu Q, Liu S, Huan Y, Wang X, Shen Z (2018) Maltol, a food flavor enhancer, attenuates diabetic peripheral neuropathy in streptozotocin-induced diabetic rats. Food Funct 9(12):6287–6297. https://doi.org/10.1039/C8FO01964A
Henning RJ (2018) Type-2 diabetes mellitus and cardiovascular disease. Future Cardiol 14(6):491–509. https://doi.org/10.2217/fca-2018-0045
Hoang HTN, Dinh TTT, Pham TV, Le HBT, Ho DV (2020) Chemical composition and acetylcholinesterase inhibitory activity of essential oil from rhizomes of *Distichochlamys benenica*. Hue Univ J Sci Nat Sci 129(1D):43–49
Hossain TJ, Harada Y, Hirayama H, Tomotake H, Seko A, Suzuki T (2016) Structural analysis of free *N*-glycans in α-glucosidase mutants of *Saccharomyces cerevisiae*: lack of the evidence for the occurrence of catabolic α-glucosidase acting on the *N*-glycans. PLoS ONE 11(3):e0151891. https://doi.org/10.1371/journal.pone.0151891
Medical Publishing House (2017) Vietnamese Pharmacopoeia V, Hanoi
Huong LT, Chau DT, Hung NV, Dai DN, Ogunwande IA (2017) Volatile constituents of Distichochlamys citrea MF Newman and Distichochlamys orlowii K Larsen MF Newman (Zingiberaceae) from Vietnam. J Med Plants Res 11(9):188–193. https://doi.org/10.5897/JMPR2016.6337
Ito F, Sono Y, Ito T (2019) Measurement and clinical significance of lipid peroxidation as a biomarker of oxidative stress: oxidative stress in diabetes, atherosclerosis, and chronic inflammation. Antioxidants 8(3):72. https://doi.org/10.3390/antiox8030072
Kang KS, Yamabe N, Kim HY, Yokozawa T (2008) Role of maltol in advanced glycation end products and free radicals: in-vitro and in-vivo studies. J Pharm Pharmacol 60(4):445–452. https://doi.org/10.1211/jpp.60.4.0006
Kapetanovic IM (2008) Computer-aided drug discovery and development (CADDD): *in silico*-chemico-biological approach. Chem BioL Interact 171(2):165–176. https://doi.org/10.1016/j.cbi.2006.12.006
Kharkyanen VN, Petrov EG, Ukrainskii II (1978) Donor-acceptor model of electron transfer through proteins. J Theor Biol 73(1):29–50. https://doi.org/10.1016/0022-5193(78)90178-9
Koopmans T (1934) Über die Zuordnung von Wellenfunktionen und Eigenwerten zu den einzelnen Elektronen eines Atoms. Physica 1(1–6):104–113. https://doi.org/10.1016/S0031-8914(34)90011-2
Kowalski S, Lukasiewicz M, Duda-Chodak A, Ziec G (2013) 5-Hydroxymethyl-2-furfural (HMF)–heat-induced formation, occurrence in food and biotransformation-a review. Polish J Food Nutr Sci 63(4):207–225. https://doi.org/10.2478/v10222-012-0082-4
Lipinski CA, Lombardo F, Dominy BW, Feeney PJ (1997) Experimental and computational approaches to estimate solubility and permeability in drug discovery and development settings. Adv Drug Deliv Rev 23(1–3):3–25. https://doi.org/10.1016/S0169-409X(96)00423-1
Loan HTP, Bui TQ, My TTA, Hai NTT, Quang DT, Tat PV, Nhung NTA (2020) In-depth investigation of a donor-acceptor interaction on the heavy-group-14@ group-13-diyls in transition-metal tetrylone complexes: structure, bonding, and property. ACS Omega 5(33):21271–21287. https://doi.org/10.1021/acsomega.0c03237
Marković ZS, Dimitrić Marković JM, Milenković D, Filipović N (2011) Mechanistic study of the structure–activity relationship for the free radical scavenging activity of baicalein. J Mol Model 17(10):2575–2584. https://doi.org/10.1007/s00894-010-0942-y
Mazumder J, Chakraborty R, Sen S, Vadra S, De B, Ravi TK (2009) Synthesis and biological evaluation of some novel quinoxalinyl triazole derivatives. Der Pharma Chem 1:188–198
Moradi-Marjaneh R, Paseban M, Sahebkar A (2019) Natural products with SGLT2 inhibitory activity: possibilities of application for the treatment of diabetes. Phyther Res 33(10):2518–2530. https://doi.org/10.1002/ptr.6421
Mošovská S, Nováková D, Kaliňák M (2015) Antioxidant activity of ginger extract and identification of its active components. Acta Chimica Slovaca 8(2):115–119. https://doi.org/10.1515/acs-2015-0020
Moteki H, Hibasami H, Yamada Y, Katsuzaki H, Imai K, Komiya TAKASHI (2002) Specific induction of apoptosis by 1,8-cineole in two human leukemia cell lines, but not a in human stomach cancer cell line. Oncol Rep 9(4):757–760. https://doi.org/10.3892/or.9.4.757
Newman MF (1995) *Distichochlamys*, a new genus from Vietnam. Edinburgh J Bot 52(1):65–69. https://doi.org/10.1017/S0960428600000192X
Newsholme P, Cruzat VF, Keane KN, Carlessi R, de Bittencourt Jr PIH (2016) Molecular mechanisms of ROS production and oxidative stress in diabetes. Biochem J 473(24):4527–4550. https://doi.org/10.1042/BCJ20160503C
Ngo TD, Tran TD, Le MT, Thai KM (2016) Computational predictive models for P-glycoprotein inhibition of in-house chalcone derivatives and drug-bank compounds. Mol Divers 20(4):945–961. https://doi.org/10.1007/s11030-016-9688-5
Oguntibeju OO (2019) Type 2 diabetes mellitus, oxidative stress and inflammation: examining the links. Int J Physiol Pathophysiol Pharmacol 11(3), 45. PMID: 31333808; PMCID: PMC6628012
Pham TV, Hoang HNT, Nguyen HT, Nguyen HM, Huynh CT, Vu TY, Do BH (2021) Anti-inflammatory and antimicrobial activities of compounds isolated from *Distichochlamys benenica*. Biomed Res Int. https://doi.org/10.1155/2021/6624347
Pires DE, Blundell TL, Ascher DB (2015) pkCSM: predicting small-molecule pharmacokinetic and toxicity properties using graph-based signatures. J Med Chem 58(9):4066–4072. https://doi.org/10.1021/acs.jmedchem.5b00104
Quintans-Júnior LJ, Guimarães AG, Santana MTD, Araújo BE, Moreira FV, Bonjardim LR, Santos MR (2011) Citral reduces nociceptive and inflammatory response in rodents. Rev Bras Farmacogn 21(3):497–502. https://doi.org/10.1590/S0102-695X2011005000065
Rad AS, Ardjmand M, Esfahani MR, Khodashenas B (2021) DFT calculations towards the geometry optimization, electronic structure, infrared spectroscopy and UV–vis analyses of Favipiravir adsorption on the first-row transition metals doped fullerenes; a new strategy for COVID-19 therapy. Spectrochim Acta Part A Mol Biomol Spectrosc 247:119082. https://doi.org/10.1016/j.saa.2020.119082
Radi R, Denicola A, Morgan B, Zielonka J (2018) Foreword to the free radical biology and medicine special issue on¨ Current fluorescence and chemiluminescence approaches in free radical and redox biology¨.Free Radic Biol Med 128, 1–2. https://doi.org/10.1016/j.freeradbiomed.2018.09.027
Reed AE, Weinstock RB, Weinhold F (1985) Natural population analysis. J Chem Phys 83(2):735–746. https://doi.org/10.1063/1.449486
Rehder D (2020) The potentiality of vanadium in medicinal applications. Inorganica Chim Acta 504:119445. https://doi.org/10.1016/j.ica.2020.119445
Reid TS (2013) Practical use of glucagon-like peptide-1 receptor agonist therapy in primary care. Clin Diabetes 31(4):148–157. https://doi.org/10.2337/diaclin.31.4.148
Rosenberg B (1962) Electrical conductivity of proteins. Nature 193(4813):364–365. https://doi.org/10.1038/193364a0
Sagaama A, Noureddine O, Brandán SA, Jarczyk-Jędryka A, Flakus HT, Ghalla H, Issaoui N (2020) Molecular docking studies, structural and spectroscopic properties of monomeric and dimeric

species of benzofuran-carboxylic acids derivatives: DFT calculations and biological activities. Comput Biol Chem 87:107311. https://doi.org/10.1016/j.compbiolchem.2020.107311

Sandholm N, Forsblom C (2020) Genetics of diabetic microvascular disease. Microvasc Dis Diabetes. https://doi.org/10.1002/9781119309642.ch3

Sha JY, Zhou YD, Yang JY, Leng J, Li JH, Hu JN, Li W (2019) Maltol (3-hydroxy-2-methyl-4-pyrone) slows D-galactose-induced brain aging process by damping the Nrf2/HO-1-mediated oxidative stress in mice. J Agric Food Chem 67(37):10342–10351. https://doi.org/10.1021/acs.jafc.9b04614

Shobana S, Vidhya VG, Ramya M (2009) Antibacterial activity of garlic varieties (ophioscordon and sativum) on enteric pathogens. Curr Res J Biol Sci 1(3):123–126

Song Y, Hong S, Iizuka Y, Kim CY, Seong GJ (2015) The neuroprotective effect of maltol against oxidative stress on rat retinal neuronal cells. Korean J Ophthalmol 29(1):58–65. https://doi.org/10.3341/kjo.2015.29.1.58

Sun F, Chai S, Yu K, Quan X, Yang Z, Wu S, Shi L (2015) Gastrointestinal adverse events of glucagon-like peptide-1 receptor agonists in patients with type 2 diabetes: a systematic review and network meta-analysis. Diabetes Technol Ther 17(1):35–42. https://doi.org/10.1089/dia.2014.0188

Sun H, Saeedi P, Karuranga S, Pinkepank M, Ogurtsova K, Duncan BB, Magliano DJ (2022) IDF diabetes atlas: Global, regional and country-level diabetes prevalence estimates for 2021 and projections for 2045. Diabetes Res Clin Pract 183:109119. https://doi.org/10.1016/j.diabres.2021.109119

Suresh BV (2010) Solid state devices and technology. Pearson Education, India

Tarasova O, Poroikov V, Veselovsky A (2018) Molecular docking studies of HIV-1 resistance to reverse transcriptase inhibitors: mini-review. Molecules 23(5):1233. https://doi.org/10.3390/molecules23051233

Thai KM, Le DP, Tran TD, Le MT (2015) Computational assay of Zanamivir binding affinity with original and mutant influenza neuraminidase 9 using molecular docking. J Theor Biol 385:31–39. https://doi.org/10.1016/j.jtbi.2015.08.019

Thao TTP, Bui TQ, Hai NTT, Huynh LK, Quy PT, Bao NC, Nhung NTA (2021a) Newly synthesised oxime and lactone derivatives from *Dipterocarpus alatus* dipterocarpol as anti-diabetic inhibitors: experimental bioassay-based evidence and theoretical computation-based prediction. RSC Adv 11(57):35765–35782. https://doi.org/10.1039/d1ra04461c

Thao TTP, Bui TQ, Quy PT, Bao NC, Van Loc T, Van Chien T, Nhung NTA (2021b) Isolation, semi-synthesis, docking-based prediction, and bioassay-based activity of *Dolichandrone spathacea* iridoids: new catalpol derivatives as glucosidase inhibitors. RSC Adv 11(20):11959–11975. https://doi.org/10.1039/D1RA00441G

Tomasik P, Horton D (2012) Enzymatic conversions of starch. Adv Carbohyd Chem Biochem 68:59–436. https://doi.org/10.1016/B978-0-12-396523-3.00001-4

Tripathi UN, Chandra D (2009) The plant extracts of *Momordica charantia* and *Trigonella foenum graecum* have antioxidant and anti-hyperglycemic properties for cardiac tissue during diabetes mellitus. Oxid Med Cell Longev 2(5):290–296. https://doi.org/10.4161/oxim.2.5.9529

Ty PV, Hoai NT, Khan NV, Duc HV (2017) Chemical composition of the essential oils of *Distichochlamys cetria* leaves collected from central Vietnam. Vietnam J Chem 55(4E23):358–362

Vinothiya K, Ashokkumar N (2017) Modulatory effect of vanillic acid on antioxidant status in high fat diet-induced changes in diabetic hypertensive rats. Biomed Pharmacother 87:640–652. https://doi.org/10.1016/j.biopha.2016.12.134

Wang Q, Wang J, Li N, Liu J, Zhou J, Zhuang P, Chen H (2022) A systematic review of orthosiphon stamineus benth in the treatment of diabetes and its complications. Molecules 27(2):444. https://doi.org/10.3390/molecules27020444

Weigend F, Ahlrichs R (2005) Balanced basis sets of split valence, triple zeta valence and quadruple zeta valence quality for H to Rn: design and assessment of accuracy. Phys Chem Chem Phys 7(18):3297–3305. https://doi.org/10.1039/b508541a

Wu Y, Ding Y, Tanaka Y, Zhang W (2014) Risk factors contributing to type 2 diabetes and recent advances in the treatment and prevention. Int J Med Sci 11(11):1185. https://doi.org/10.7150/ijms.10001

Xiao J (2022) Recent advances in dietary flavonoids for management of type 2 diabetes. Curr Opin Food Sci. https://doi.org/10.1016/j.cofs.2022.01.002

Yaribeygi H, Sathyapalan T, Atkin SL, Sahebkar A (2020) Molecular mechanisms linking oxidative stress and diabetes mellitus. Oxid Med Cell Longev. https://doi.org/10.1155/2020/8609213

Zhao L, Chen J, Su J, Li L, Hu S, Li B, Chen T (2013) In vitro antioxidant and antiproliferative activities of 5-hydroxymethylfurfural. J Agric Food Chem 61(44):10604–10611. https://doi.org/10.1021/jf403098y